Aerospace Science and Technology 178 (2026) 112452

Contents lists available at ScienceDirect

Aerospace Science and Technology

journal homepage: www.elsevier.com/locate/aescte

Original article

No-return disposal trajectories in the Earth-Moon system: A parametric analysis

Mathilda Bolis [a,*], Elisa Maria Alessi [b], Camilla Colombo [a]

[a] Dipartimento di Scienze e Tecnologie Aerospaziali (DAER), Politecnico di Milano, Via La Masa, 34, Milano, 20156, Italy
[b] Istituto di Matematica Applicata e Tecnologie Informatiche "Enrico Magenes", Consiglio Nazionale delle Ricerche, Via Alfonso Corti 12, Milano, 20133, Italy

ARTICLE INFO

Communicated by Chaoyong Li

Keywords:
Earth-Moon system
Circular restricted three body problem
End-of-life disposal design
Escape no-return trajectories
Dynamical cartography

ABSTRACT

The growing interest in cislunar space shown in recent years, together with the increasing number of studies on missions targeting the Earth-Moon (EM) system, has raised numerous questions, both on how to operate such missions safely and on how to prevent the emergence of a debris problem in the region. The exponential growth in the number of objects orbiting near Earth has already threatened its long-term sustainability: it is necessary to prevent this from happening in the cislunar domain as well, which is additionally characterised by strong non-linear dynamics. The most effective way to mitigate the problem is to prevent it from happening in the first place, which can be achieved by developing efficient, robust and economically attractive End-of-Life (EoL) disposal solutions.

This work investigates the dynamical behaviours of unstable manifold trajectories departing from Libration Point Orbits (LPOs) considered of interest for future cislunar missions. To understand how these can be leveraged on would then be the foundation of efficient disposal design. The objective is to identify how unstable manifold trajectories' behaviours can be exploited to improve the cost-effectiveness, efficiency, and reliability of EoL disposal strategies when included in a more comprehensive study, performing a parametric analysis on various families of periodic orbits, developing maps that would allow operators, given certain constraints, to identify possible disposal options based on maximum Time of Flight (ToF) and available on-board fuel. To do so, unstable manifold trajectories of various periodic orbits, evaluated at different departure phase angles, are propagated for a maximum time of six months. Possible outcomes of propagation include crossing EM-L_2, impacting the Moon, intersecting an orbit around the Earth with a radius equal to that of the Geostationary (GEO) belt or remaining within the Zero Velocity Curves (ZVCs) of the EM system for the overall time frame considered. If the first outcome is achieved, the focus shifts to no-return escape trajectories from EM-L_2. After escape through the EM-L_2 bottleneck, a manoeuvre is applied to modify the trajectory's energy so that the EM system's ZVCs close, preventing the satellite from re-entering their inner region. The analysis is repeated for seven distinct families of LPOs: the Halo, Lyapunov and Vertical families in both EM-L_1 and L_2, together with the Butterfly family. The results of this work are maps showing how the trajectories evolve as a function of the phase angle of the starting point and its Jacobi Constant (JC), representing a preliminary dynamic cartography of escape behaviour in the EM system.

List of acronyms

Acronym	Description
CoM	Centre of mass
CR3BP	Circular Restricted Three Body Problem
EM	Earth-Moon
EoL	End-of-Life
GEO	Geostationary Orbit
JC	Jacobi Constant
L_i	i-th Lagrangian point
LPO	Libration Point Orbit
NRHO	Near Rectilinear Halo Orbit
SE	Sun-Earth
ToF	Time of Flight
ZVC	Zero Velocity Curve

* Corresponding author.
E-mail addresses: mathilda.bolis@polimi.it (M. Bolis), em.alessi@mi.imati.cnr.it (E.M. Alessi), camilla.colombo@polimi.it (C. Colombo).

https://doi.org/10.1016/j.ast.2026.112452
Received 1 December 2025; Received in revised form 23 March 2026; Accepted 23 April 2026
Available online 2 May 2026

1. Introduction

In recent years, there has been a renewed interest from the international community towards the cislunar region, defined as an area of space extending approximately from hyper-Geostationary Orbits (GEOs) up to the Lagrangian points of the Earth-Moon (EM) system, as stated, for example, in [1]. Several missions targeting this region are planned for the near future, such as those within the Artemis program.

This renewed interest coincides with the growing complexity of the near-Earth space debris problem. As discussed in [2], the large number of satellites launched in recent decades has led to an exponential increase in the population of objects in orbit, posing risks to the current and future access to space. This led to the growing awareness that, much like any other terrestrial ecosystem, space is a finite and fragile resource and, as such, requires active preservation to ensure that future generations can continue to benefit from its use. Translating this principle into concrete actions, however, remains a considerable challenge, and numerous studies are currently devoted to developing effective strategies for mitigating the debris problem.

It is not difficult to imagine that a similar issue could arise in cislunar space as well, especially given the renewed global interest in this region. Cislunar dynamics is also inherently more unstable and non-linear than near-Earth dynamics, meaning that any debris-related problem in an area strongly influenced by both the Earth's and the Moon's gravity would be far more challenging to handle than what has been seen in near-Earth space. In this context, the need for a dedicated cislunar space situational awareness infrastructure becomes evident. Building on the experience gained in Earth's environment, this would provide the tools necessary to prevent debris-related issues or, at least, support their effective management. A growing number of studies are emerging on these topics in the last few years; among them, just to cite some examples, are [3] and [4].

One of the most effective mitigation strategies is to include End-of-Life (EoL) disposal procedures in the mission design phases, thereby preventing the problem of space debris from arising in the first place. According to the European Space Agency Space Debris Mitigation Working Group [5], missions in the EM system should consider four disposal strategies, listed in order of preference: "heliocentric disposal, lunar impact, Earth re-entry, and lunar graveyard orbit". The selection of a specific disposal option must be supported by detailed analyses, including numerical propagation within a realistic dynamical model. Moreover, disposal trajectories should be evaluated over a minimum time of 100 years to assess the probability of Earth re-entry or lunar impact, as well as to identify the associated impact regions. Strong interest in this topic has been demonstrated in recent years by both companies and international agencies. Many have recently conducted preliminary assessments to evaluate the effectiveness and cost of each disposal strategy, review the set of regulations developed to date, and attempt to determine which option may be the most advantageous [6–9].

Heliocentric disposal consists of designing a trajectory that moves from a periodic orbit in the EM system to L_1 or, preferably, L_2 of the Sun-Earth (SE) system. Once the spacecraft has crossed the bottleneck region near SE-L_1 or SE-L_2, the spacecraft can either be considered effectively disposed of, i.e., placed on a heliocentric trajectory, requiring only long-term simulations to ensure that it does not re-enter the inner region of the SE Zero Velocity Curves (ZVCs) for at least 100 years, or, if a stricter safety requirement is to be enforced, a second manoeuvre may be used to close the SE-ZVCs, thereby preventing the satellite from re-entering their inner region. In [10], an energetic approach is applied to the unstable manifolds of SE-L_2 Libration Point Orbits (LPOs) escaping from SE-L_2 to close the ZVCs. This strategy is also applied in [11] and [12] to the EoL design for GAIA, operating on an LPO in SE-L_2. In [13], the effect of solar radiation pressure on heliocentric dynamics is studied to derive EoL low-cost solutions for the same mission. In the EM system, heliocentric disposal was applied in [14] to the Near Rectilinear Halo Orbit (NRHO) chosen as a baseline for the Lunar Gateway. Escape dynamics from the same reference NRHO have also been extensively studied in works such as [15], [16], and [17], with a particular focus on the magnitude of the minimum impulse guaranteeing robust escape from the system when departing from perilune and on metrics defining escape for certain escape trajectories. Heliocentric disposal has also been considered for the Halo and Lyapunov orbital families in [18], in which a preliminary analysis on the use of electric propulsion for disposal in the context of the EM Circular Restricted Three Body Problem (CR3BP) was presented.

Lunar impact and Earth impact consist of designing trajectories targeting a collision with one of the two celestial bodies, while the lunar graveyard orbit option consists of inserting the spacecraft into a stable orbit in the EM system, in which the evolution of the object remains constrained for at least 100 years. Such orbits may be either distant retrograde orbits or those located near the L_4 or L_5 Lagrange points of the EM system. For a visual representation of all four disposal options, the reader is referred to [6]. In [19], the reachability of each of the four possible disposal outcomes was evaluated as a function of the initial impulse magnitude, applied in the local velocity direction, and the departure phase angle for one EM-L_2 Halo and one NRHO.

In this work, the design of disposal strategies for satellites operating in cislunar space is addressed primarily from a dynamical perspective. The focus is to investigate whether specific behaviours within the EM-CR3BP can be exploited to enable low-cost disposal solutions. In particular, we focus on the study of unstable manifold escape trajectories that, for a satellite departing from an EM periodic orbit, evolve toward the EM-L_2 region. Once the spacecraft reaches the outer side of the ZVCs of the EM system, these are virtually closed, making it impossible for the spacecraft to re-enter cislunar space. This approach allows for the definition of a disposal strategy that considers cislunar space as the "safe zone" in which disposed spacecraft should not re-enter.

A parametric analysis is then carried out, considering seven families of periodic orbits deemed particularly relevant for future cislunar missions: the Halo, Lyapunov and Vertical families in both EM-L_1 and L_2, together with the Butterfly family. Analysing them all provides an opportunity to create a preliminary map of the costs required to place a spacecraft leaving cislunar space on an escape trajectory and to study many behaviours characteristic of a three-body dynamical system. The aim is to identify the minimum ΔV required to dispose of the spacecraft with this strategy, as a function of the Jacobi Constant (JC) of the departure orbit and the phase angle of the point along it at which the spacecraft is injected in the unstable manifold. The obtained results highlight both dynamical behaviours of interest within the EM three-body problem, which can be leveraged on in search for low-cost disposal solutions, and practical insights showing how, given mission constraints such as available disposal budget on board and Time of Flight (ToF) dedicated to the EoL phase, viable and effective disposal solutions can be identified. The outcome of this work is a set of maps providing a preliminary dynamic cartography of cislunar space. These maps can eventually allow operators to select potential disposal solutions while taking into account the periodic operational orbit, the ΔV available on-board, and the maximum ToF. The novelty of this study lies in the systematic characterisation of unstable manifold escape dynamics in the EM system, combining parametric maps with a detailed dynamical interpretation of the underlying mechanisms, analysing cislunar escape trajectories from both a parametric and a dynamical perspective and exploring their applicability to cislunar disposal strategies.

Finally, it is essential to note that, according to the lunar space debris mitigation guidelines defined in [5], the disposal phase is considered complete only when the spacecraft is in the exterior region of the SE system, not just the EM one. However, it is considered worthwhile to study the dynamics that characterise EM-L_2 escape no-return trajectories to better understand which parameters influence the disposal dynamics and costs. In a second phase, the analysis will be extended to trajectories that escape from SE-L_2 and do not re-enter the inner region of the SE system within 100 years.

2. Circular restricted three body problem

The motion of a massless object subject to the gravitational attraction of two major bodies, say the Earth and the Moon, can be approximated through the CR3BP [20]. The primaries orbit in circular motion around their common Centre of Mass (CoM) in a rotating and dimensionless reference frame, with the z-axis perpendicular to their orbital plane, the x-axis chosen as the line connecting the major primary to the minor, and the y-axis completing the right-handed tern. Position and velocity of a massless object are denoted as $\boldsymbol{r} = [r_x, r_y, r_z]$ and $\boldsymbol{v} = [v_x, v_y, v_z]$. The equations of motion describing CR3BP dynamics in the rotating reference frame can be expressed as follows:

$$\begin{cases} \dot{\boldsymbol{r}} = \boldsymbol{v} \\ \dot{\boldsymbol{v}} = 2\begin{bmatrix} v_y \\ -v_x \\ 0 \end{bmatrix} + \nabla_{\boldsymbol{r}} U \end{cases} \tag{1}$$

where the potential-like function U is defined as:

$$U(\boldsymbol{r}) = \frac{1}{2}(r_x^2 + r_y^2) + \frac{1-\mu}{r_1} + \frac{\mu}{r_2} + \frac{1}{2}\mu(1-\mu) \tag{2}$$

Within this framework, lengths are scaled with respect to the average EM distance, 384399 km, and times so that the mean motion of the rotating frame equals 1. Dimensionless lengths are represented by the unit ndL, and dimensionless times by the unit ndT. The dimensionless gravitational constant for the EM system is denoted by μ and has a value of 0.01215. The variables r_1 and r_2 represent, respectively, the distances between the third body and each of the primaries, given that the Earth is located at $x = -\mu$ and the Moon at $x = 1 - \mu$.

In the CR3BP, a singular integral of motion is definable. A version of this integral, referred to as the JC, is expressed as follows:

$$JC(\boldsymbol{r}, \boldsymbol{v}) = 2\bar{U}(\boldsymbol{r}) - ||\boldsymbol{v}||^2 \tag{3}$$

where $\bar{U}(\boldsymbol{r})$ is equal to $U(\boldsymbol{r})$ minus the constant term. The JC is dependent on the spacecraft's state and can be associated with an energy-like constant. An increase in JC results in a reduction in the system's energy, and vice versa, since, when the equations of motion for the CR3BP are derived using a Hamiltonian approach, a constant representing the total mechanical energy can be defined as $E = -JC/2$.

Five equilibrium points of the CR3BP can be found: the libration or Lagrange points $L_1 - L_5$. Three of these lie on the x-axis of the rotating reference frame ($L_1 - L_3$, collinear Lagrange points), while the remaining two (L_4 and L_5, triangular Lagrange points) form the vertices of an equilateral triangle together with the minor primary.

For this discussion, what is of particular interest is that the possible motion of a massless particle with respect to Lagrangian points can be classified according to its energy. In the spatial CR3BP, for a fixed energy level E_0, it is possible to define a five-dimensional energy surface embedded in a six-dimensional phase space. The possible regions of motion for a massless object with energy E_0 in a system with gravitational constant μ are defined by projecting the energy surface into the position space of the rotating system. This region is historically known as the Hill region, and its boundaries as ZVCs, which are identified as the locus of points at which the kinetic energy of the massless particle is zero [21].

To a fixed JC level, JC_0, corresponds the fixed energy level E_0. Since Eq. (3) holds, it is possible to find that for any massless object subject to the CR3BP dynamics, it has to always be true that $2\bar{U}(\boldsymbol{r}) \geq JC(\boldsymbol{r}, \boldsymbol{v})$. The boundary condition, such that the velocity of the massless object is zero, is represented by the Equation $2\bar{U}(\boldsymbol{r}) = JC_0$, which identifies the ZVCs of the system given a certain energy level E_0.

Regions of space in which the inequality does not hold are instead designated as forbidden regions, that is, areas in which the motion of the third body is not permitted. In the context of motion being constrained to the plane of the primaries, the ZVCs result in a curve forming a barrier that the massless third body is unable to cross in planar position space.

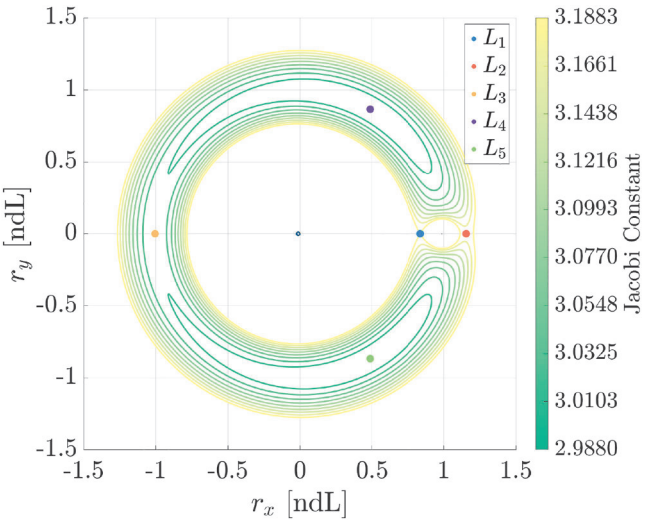

Fig. 1. Libration points and ZVC as a function of JC in the planar CR3BP - EM system.

In Fig. 1, the location of the five Libration points of the EM system is pictured, together with the planar ZVCs as a function of the value of JC considered.

When the energy of a massless particle changes, its regions of possible motion also change. Of particular interest is that as a particle's energy varies, its motion in the bottleneck regions near the $L_1 - L_2$ collinear libration points becomes either allowed or forbidden. Fig. 2 shows the ZVCs of a particle subject to CR3BP dynamics in the EM system at three different energy levels. As the energy of the massless particle decreases and its JC increases, the bottleneck region near L_1 or L_2 closes. This makes it impossible for an object orbiting near the Moon to reach the outer region of the ZVCs and, likewise, for an object orbiting in the outer region to reach the vicinity of the Earth or the Moon. The JC boundary value for which the bottleneck region closes in L_2 is identified as JC_{L_2}, that for which it closes in L_1 as JC_{L_1}. It follows that, for $JC > JC_{L_2}$, the bottleneck region in L_2 is closed [10].

3. Periodic orbits

In addition to equilibrium points, CR3BP solutions also include periodic orbits. Families of periodic orbits either stem from one of the Libration points defined above or, secondarily, from other families of periodic orbits, as described in [22]. A Newton-like differential correction method is used to generate periodic solutions, while numerical continuations are employed to find members of the families which are increasingly distant from the bifurcation point. To find a solution, both periodicity and orthogonality must be enforced. This means that:

- To enforce periodicity, a state $\boldsymbol{x} = [\boldsymbol{r}, \boldsymbol{v}]$ must recur after a period.
- To enforce orthogonality, periodic orbits must be symmetric with respect to the xz-plane (or the x-axis if the periodic orbit under analysis is planar) and must intersect this plane orthogonally.

The link between a given initial state and an ideal final state whose desired characteristics are known can be established by imposing these two conditions: the differential correction algorithm adjusts the initial state so that the final one is as desired, as shown in [21]. Through this procedure, initial conditions generating a periodic orbit are defined. Once a solution is found, the process is repeated to find other members of the same family thanks to continuation methods.

Dozens of families of periodic orbits can be defined in the CR3BP dynamical framework. For the analysis of escape trajectories from EM-L_2, this paper considers only seven: the Halo, Lyapunov and Vertical families in both L_1 and L_2, and the Butterfly family. For both the Halo and

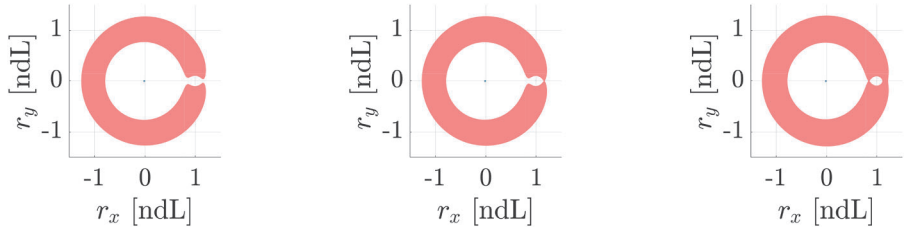

Fig. 2. ZVCs in the EM system for various values of Jacobi's constant. From left to right: $JC = 3.1671$; $JC = 3.1721$, corresponding to the JC at L_2; $JC = 3.1883$, corresponding to the JC at L_1.

Butterfly families, the southern branch is considered. These families of orbits are chosen primarily because of their high relevance to current and future missions.

Families of orbits in which most members are linearly stable, such as the Hénon families f and g, are not considered. This choice is made because the techniques used to design escape trajectories inherently rely on the instability of the departure periodic orbit, as will be detailed in the following Sections. This also holds for the families of orbits analysed, where linearly stable or quasi-stable members, that is, with a stability index less than or equal to one [23], are discarded from the analysis.

For each family considered, 30 members were selected for the parametric analysis, with a JC ranging from about 3.15 to about 3. The upper limit of the JC interval is fixed by knowing that $JC_{L_2} = 3.1721$. Escape trajectories from L_2 for satellites with energy levels lower than or close to that of the second Lagrange point are not considered because opening the ZVCs at L_2 before escaping and closing them afterwards would be required, which is not taken into account in this work. Instead, the lower limit of the energy range is set because features along the various orbit families behave differently for values of JC lower than 3 with respect to the range considered. Note that, for the Halo families, only the branch in which JC decreases as the minimum distance from the Moon decreases was taken into account. Namely, as shown in [24], the analysis did not consider NRHOs.

The same energy range was chosen for all families except for the Butterfly one, whose JC ranges from 3.09 to 3.07. For this family, orbits with JC values higher than about 3.09 can be computed mathematically but have no physical meaning, as they intersect the Moon. Orbits with lower JC values do exist, but their shape differs substantially from that of the orbits in the chosen range [25], making them difficult to use in future applications. Moreover, they exhibit characteristics that differ from those of the other orbits considered.

All elements selected for the analysis are represented in Fig. 3 as a function of the phase angle, which is defined as:

$$\theta = \frac{2\pi t}{T} \tag{4}$$

where T is the orbital period and t is the propagation time. In Fig. A.33, the same orbits are represented as a function of the distance from the Moon, which is also related to the evolution of θ. In both Figures, the blue dot represents the Lagrangian point L_1, the red dot L_2.

By analysing how the phase angle evolves across different families of orbits, it is observed that this parameter follows a similar behaviour both for the Halo and Lyapunov families. The distance between a point along the orbit and the Moon consistently lowers at phase angles about 180°, and increases at about 0° and 360°. For the planar case, the only inconsistency with respect to the spatial one is that, when considering orbits far from the Lagrangian point from which they bifurcate, the distance from the Moon decreases slightly at 0° before reaching its maximum around 90°. Anyway, the evolution of the phase angle and the distance from the Moon is similar in all four cases.

For the Vertical and Butterfly families, the phase angle trend is not consistently correlated with the one defining the distance from the Moon. This is due both to the way the phase angle is defined for these families and their characteristics: their geometry makes it difficult to establish a clear relationship between the two parameters.

The trend of JC as a function of the quantity d_A is shown in Fig. 4 for the seven families considered. The parameter d_A represents the distance between:

- the point with negative r_z identifying the intersection between the xz-plane and the orbit, i.e. the apolune, and L_i for the Halo and Lyapunov families centred at L_i, $i = 1, 2$,
- the point identifying the intersection between the xy-plane and the orbit, and L_i for the Vertical family centred at L_i, $i = 1, 2$,
- the point closer to L_1 identifying the intersection between the xz-plane and the orbit, and the Moon for the Butterfly family.

Note that all the points on the orbits from which the quantity d_A is measured are those identified by $\theta = 0°$.

This quantity is of particular interest, since for the Halo, Lyapunov, and Vertical families, the i-th Lagrange point L_i represents the equilibrium point about which the corresponding periodic orbits are defined. The Butterfly family, on the other hand, develops around the Moon, and it is generated by a period-doubling bifurcation of the L_2 Halo family as shown in [25]. In this case, the quantity d_B is computed as the distance between the Moon and the point at which the orthogonality condition for the definition of the periodic orbits is applied.

In Fig. 4, the evolution of the stability index, a measure of the linear stability of a periodic orbit, and the perilune radius, computed as the minimum distance from the Moon reached on a periodic orbit, are also represented as a function of the quantity d_A.

In Fig. 4, elements chosen for the analysis are highlighted by a filled dot, and are selected by sampling equally spaced values of JC in the chosen interval. Note that, within these energy ranges, none of the members of the families encounters the Moon. Also, the trend of JC along each of the families is consistent with that of the perilune radius and the stability index: as JC decreases along a single family, the stability index and the perilune radius decrease too, and orbits approach the Moon.

4. Modelling escape no-return disposal trajectories

No-return disposal trajectories are defined as orbits leaving cislunar space by passing through EM-L_2 so that they are guaranteed to at least theoretically remain outside the EM vicinity for at least 100 years. This involves designing two-impulse disposal trajectories in which the first impulse, ΔV_1, is given at the periodic orbit, in the direction of its unstable manifold, to move the satellite away from its reference trajectory, and the second impulse, ΔV_2, is given in anti-tangential to the local velocity direction and is used to close the ZVCs once outside EM-L_2, to prevent the spacecraft from returning in the EM neighbourhood. To summarise, no-return disposal trajectories are designed according to the schema illustrated in Fig. 5.

Initially, simulations are performed within the CR3BP framework. Subsequent validation involves verifying the spacecraft remains outside cislunar space over at least a 100-year period when employing the n-body dynamical model for propagation. The upcoming Sections offer a comprehensive explanation of the design process for the two-impulse trajectory. First, the selection of ΔV_1 is outlined, then that of ΔV_2.

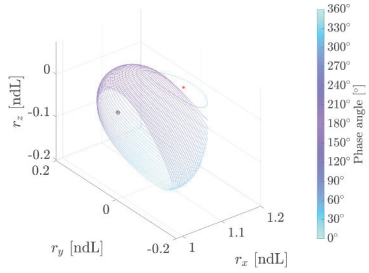

(a) EM-L_2 Halo family, southern branch.

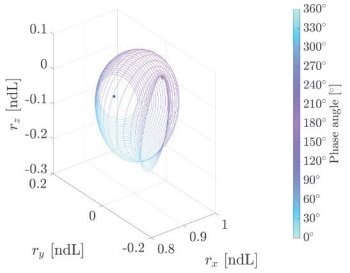

(b) EM-L_1 Halo family, southern branch.

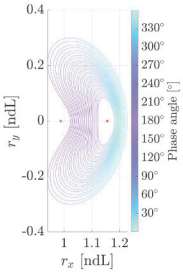

(c) EM-L_2 Lyapunov family.

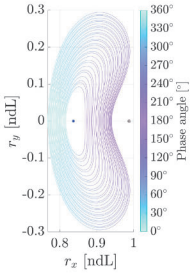

(d) EM-L_1 Lyapunov family.

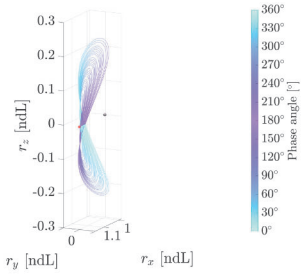

(e) EM-L_2 Vertical family.

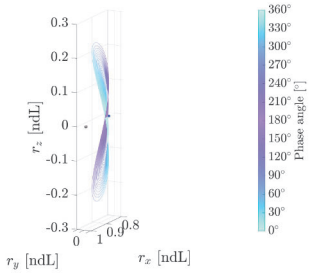

(f) EM-L_1 Vertical family.

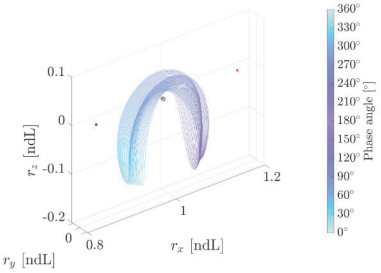

(g) Butterfly family.

Fig. 3. Periodic orbits selected for the analysis, as a function of the phase angle.

4.1. ΔV_1 selection: unstable manifolds' theory

The stable and the unstable invariant manifolds associated with a given periodic orbit are a set of trajectories that approach or depart, respectively, from the nominal orbit when propagated forward in time. The initial conditions corresponding to these trajectories can be computed thanks to the eigenvalues and eigenvectors of the monodromy matrix of the periodic orbit, which is defined as the orbit's state transition matrix evaluated after 1 orbital period. The monodromy matrix has 6 eigenvalues and, among these, the first two are equal to unity, reflecting the conservation of energy. When a linearly unstable orbit is considered, of the two remaining eigenvalue pairs, one consists of a complex conjugate couple, and one of two real and reciprocal values. This last eigenvalue couple, identified by $\lambda^{s,u}$, is such that $|\lambda^s| < 1$ and $|\lambda^u| > 1$, where the superscript s stands for *stable* and u for *unstable*. The eigenvalue λ^u corresponds to the eigenvector $\mathbf{\Lambda}^u(\theta_0)$, which is linearly tangent to the unstable manifold, i.e., the direction which asymptotically departs from the reference periodic orbit. To compute the direction of the unstable manifold at an arbitrary value of time t, hence at a generic phase angle θ:

$$\mathbf{\Lambda}^u(\theta) = \mathbf{\Phi}(t_0, t)\mathbf{\Lambda}^u(\theta_0) \tag{5}$$

where the quantity $\mathbf{\Phi}(t_0, t)$ is the state transition matrix evaluated between t_0 and t. Then, the directions found are normalised such that:

$$\hat{\mathbf{\Lambda}}^u(\theta) = \frac{\mathbf{\Lambda}^u(\theta)}{||\mathbf{\Lambda}^u(\theta)||} \tag{6}$$

In this way, following Eq. (5), a direction approximating that of the unstable manifold can be found for the overall periodic orbit considered.

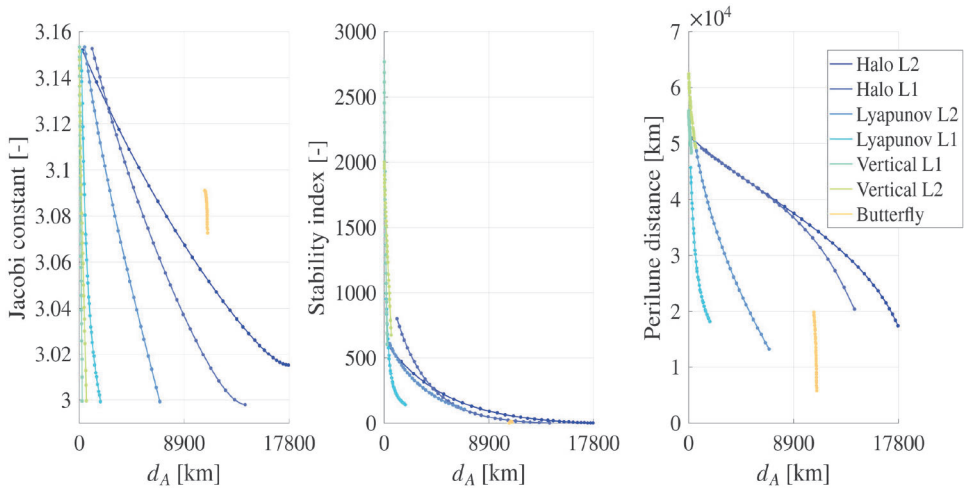

Fig. 4. Jacobi constant, stability index, and perilune radius for the different orbit families analysed, plotted as a function of the parameter d_A. Filled markers indicate the candidate orbits selected for the analysis.

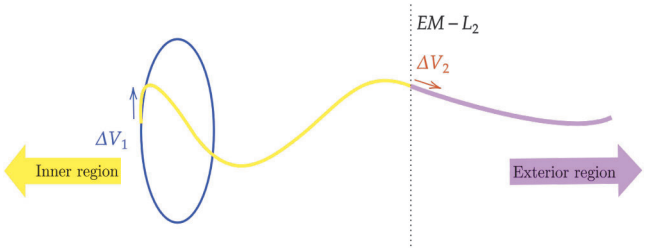

Fig. 5. No-return disposal trajectories. Schematic representation.

To determine the unstable manifold initial conditions as a function of the phase angle, a perturbation is introduced to a state of the periodic orbit along the normalised direction such that:

$$\boldsymbol{x}_0^u(\theta) = \boldsymbol{x}_0(\theta) \pm \varepsilon\, \hat{\boldsymbol{\Lambda}}^u(\theta) \tag{7}$$

For the trajectory to sensibly deviate from the periodic orbit, the perturbation ε should be considerable enough, yet it must remain sufficiently small as not to violate linearity. In the SE system, the value of ε is usually set to correspond to a displacement of 200 km between the unstable manifold initial condition and the periodic orbit considered state, given a certain value of θ, as also described in [10]. Scaling this value to the EM system results in a displacement of 250 m, equivalent to a value of ε in the order of magnitude of $1.4727 \cdot 10^{-6}$. Once the value to be given to ε is set, the magnitude of ΔV_1 is computed as the norm of the velocity variation necessary to insert the spacecraft from the periodic orbit into the unstable manifold, and is equal to about 1.4 mm/s. This leads to a difference between the JC of the reference periodic orbit and that of the unstable manifold on the order of 10^{-13}. It is important to remark that the manifold parametrisation depends on ε. This means that a change in ε is equivalent to a change in $\boldsymbol{x}_0(\theta)$, i.e., in a shift on the phase angle θ. In other words, the behaviour of the manifold trajectories shifts with respect to θ as ε varies, since a change in ε effectively shifts the reference point from which a given manifold trajectory originates. Consequently, all the results presented in the following discussion are functions of θ based on the specific choice of ε adopted.

As shown in Eq. (7), the sign of the parameter ε can be either positive or negative, and each defines a branch of the unstable manifold. As a general rule, one of the two branches leads towards the minor primary of the CR3BP system, i.e., the Moon in the case analysed, while the other heads away from it. In this application, it is the branch heading towards EM-L_2 that should be considered. It has been noted that, when analysing a single orbital family within the EM system, the branch leading the spacecraft in the desired direction is not always characterised by either a positive or a negative value of ε. Along a family of orbits, the sign of ε to be selected varies with JC. Still, when a single orbit of the family is considered, the sign of ε that results in unstable manifold trajectories moving away from the smaller primary is constant with θ. To select the relevant sign of ε for this application, both branches of the unstable manifold are initially propagated for up to six months. Then, for each of the individually considered orbits, the manifold branch heading towards EM-L_2 is selected. Propagation is carried out using a variable-step, variable-order Adams-Bashforth-Moulton predictor-corrector solver with orders ranging from 1 to 13. The relative tolerances are set to $2.22045 \cdot 10^{-14}$, and the absolute tolerances to 10^{-16}.

Once a value and a sign for ε are found, unstable manifold trajectories are propagated forward in time for up to six months. During this period, trajectories may encounter either the Moon or a sphere with a radius equivalent to that of the GEO belt around Earth, before exiting EM-L_2. Trajectories corresponding to phase angles such that this happens are discarded from further analysis. The same is true for trajectories that never leave cislunar space during the six months considered. From an operational perspective, these trajectories are not considered viable options for disposal because the highly non-linear dynamics of cislunar space make it impractical to choose disposal options involving orbiting in the EM vicinity for more than six months before disposing of the spacecraft, since the probability of uncontrolled collision in these cases would be high. These conditions are so discarded from further analysis, preferring solutions where cislunar space is rapidly left.

It is important to note that the six-month threshold was chosen as a compromise between operational needs and the necessity to adopt a time span that, being reasonably long, could highlight the trajectories' behaviour within the EM-CR3BP framework. However, it should be emphasised that the EM system dynamics have characteristic timescales that are typically much shorter than six months: for example, the period of an L_2 Halo orbit is usually about two weeks. Given the relatively long duration considered, a wide range of dynamical behaviours characteristic of escape trajectories will emerge and become evident.

4.2. ΔV_2 selection: zero velocity curves closure manoeuvres

Thanks to the first disposal manoeuvre, the trajectories reach the outer region of the ZVCs of the EM system, passing through EM-L_2. A second impulse, ΔV_2, has to be given to the spacecraft to close the ZVCs once beyond EM-L_2, to prevent it from re-entering their inner region.

This can be achieved by applying an energy-based approach to the problem and defining a manoeuvre that reduces the system's energy below the threshold at which the ZVCs are fully closed, identified as that of EM-L_2. To do so, it is sufficient to vary the JC of the orbit from JC' to JC'' so that $JC'' \geq JC_{L_2}$, as shown in e.g. [10–12], where JC' corresponds to the JC before the manoeuvre and JC'' to the one after. When this condition is verified, the ZVCs of the EM system close, as also shown in Fig. 2, and, theoretically, objects in their outer region at the time of closure are no longer able to reach their inner region. This is valid within the CR3BP dynamical framework if it is assumed that trajectories remain unperturbed after the disposal manoeuvre, i.e., their energy does not change. In a more realistic scenario, this does not apply, since the gravitational and perturbative effects of n-bodies on the system inherently change the spacecraft's energy. Disposal trajectories designed with this technique should then be validated in a more complete dynamical model to overcome this issue.

The variation in the system energy equivalent to imposing $JC'' \geq JC_{L_2}$ results in a change of the spacecraft velocity. The JC of a massless object in CR3BP is defined as in Eq. (3), and given that its position is to be considered fixed, the relationship between JC', before the manoeuvre, and JC'', after the manoeuvre, is the following:

$$JC'' = JC' + ||\boldsymbol{v}'||^2 - ||\boldsymbol{v}''||^2 \tag{8}$$

To reduce the search space for ZVC closure manoeuvres, $\boldsymbol{\Delta V_2}$ is defined tangent to the velocity direction, resulting in $v'' = v' + \Delta V_2$. This condition is substituted into Eq. (8) and, when the limiting case of $JC'' = JC_{L_2}$ is also considered, it can be shown that:

$$\Delta V_2 = -||\boldsymbol{v}'|| \pm \sqrt{||\boldsymbol{v}'||^2 - \Delta JC} \tag{9}$$

where the quantity $\Delta JC = JC_{L_2} - JC'$. The minus sign on the second part of the above equation was disregarded for further analysis, since it is typically associated with higher ΔV_2. It is important to note that an increase in the system's JC is equivalent to a decrease in its energy, meaning that the ΔV_2 calculated by this approach will always have a negative sign, i.e., the second manoeuvre is to be given tangent to the satellite's velocity, but in the opposite direction. The timing of the manoeuvre is not determined a priori, and how the results evolve based on this parameter will be addressed in the following Sections.

5. No-return escape trajectories analysis for selected L_2 and L_1 Halo orbits

The method described in the previous Sections has been applied to all the candidate orbits under consideration. The results associated with a subset of these orbits are presented in this Section to clarify which parameters influence the analysis before presenting the results of the full parametric study.

5.1. Halo in L_2, southern branch

The L_2 Halo orbit with $JC = 3.1480$ is selected as an illustrative example for the analysis, which has been performed for all the orbits identified in Section 3. The evolution of the total disposal cost associated with a spacecraft orbiting on the L_2 Halo with $JC = 3.1480$ is reported in Fig. 6.

In Fig. 6, the total cost needed to insert the spacecraft on an escape trajectory and to close the ZVCs varies as a function of the phase angle θ, which spans from 0° to 360° as introduced in Section 3, and of the time spent by the spacecraft on the manifold before performing the ZVCs closure manoeuvre, $t_{\Delta V_2}$. The departure phase angle is sampled at intervals of 3°, while the timing of the ZVC-closure manoeuvre is sampled at intervals of 1.5 days. This parameter is of interest since it is reasonable to think, as the analyses also show, that closing the ZVCs immediately once L_2 has been crossed may not be the best solution if the aim is to save as much ΔV as possible. On the other hand, from an operational perspective, a longer ToF spent by the satellite on the manifold before performing the disposal manoeuvre could introduce complications. These are not investigated extensively in this paper, which aims to define a theoretical framework for the behaviour of EM-L_2 escape disposal trajectories designed in CR3BP. However, as also stated previously, the maximum value of $t_{\Delta V_2}$ is set at six months. This choice represents a compromise between operational constraints and the need to capture key aspects of the behaviour characterising the analysed trajectories, within a scenario that remains reasonably realistic. In Fig. 6, the time $t_{\Delta V_2}$ is reported in days. The dashed black lines in the graph represent a different parametrisation of the same quantity, as a function of the EM orbital period, equal to 27.32 days. In this way, it can be observed that no clear relationship emerges between the EM rotation period, or its multiples, and the disposal cost. Having $t_{\Delta V_2} = 0$ would correspond to applying the ZVCs closure manoeuvrer simultaneously with the one used to inject the spacecraft into the selected unstable manifold.

As it is shown by the graph on the left-hand side of Fig. 6, the area close to $t_{\Delta V_2} = 0$ is almost always empty, as the satellite is, in the majority of these conditions, still in the ZVCs inner region and has not yet geometrically crossed L_2. As $t_{\Delta V_2}$ increases, and the manifold trajectories first cross L_2, the ΔV is high, to then decrease consistently for $t_{\Delta V_2} \sim 40$ days. When considering the results related to all the orbits analysed, this can be identified as a general tendency: high values of ΔV are found as soon as the satellite crosses L_2, and the escape cost decreases significantly shortly afterwards. This behaviour is clearly shown by the right-hand side of Fig. 6. It is clear that, depending on the periodic orbit considered, it could be useful to wait for about 15 to 20 days after the satellite has crossed L_2 before performing the ZVCs closure manoeuvre. Even assuming rather stringent requirements on disposal ToF, this can lead to significant propellant savings.

Anyway, the condition which has just been described does not correspond to that which minimises the total ΔV for a given θ. The coloured markers on the left side of Fig. 6 indicate this optimal state for each value of θ considered, as $t_{\Delta V_2}$ varies. If, for a given θ, the minimum ΔV is found at $t_{\Delta V_2} \geq 6$ months, the corresponding condition is not identified in Fig. 6, as this is not considered of interest for the analysis. States under which ΔV is minimised assume a parabolic-like shape as a function of the phase angle. When analyses on additional orbits are also considered, as will be shown later, it can be observed that the parabola is not always centred on the same value of θ. The colour of the markers is a function of the value of θ they are related to, defined as in the colour map used in Fig. 3.

Apart from the leftmost area in Fig. 6, others in the graph are empty too. This can occur for two main reasons:

- Under certain local conditions, the manifold's trajectories fall slightly within the ZVCs of the EM system computed for $JC = JC_{L_2}$, even though the spacecraft is far from L_2 at that instant, as can be observed from Fig. 7.

  In Fig. 7, these conditions are highlighted with a red box in the graph on the left, while on the right, the evolution of the trajectories corresponding to them is shown in the EM rotating reference frame, with the selected conditions again highlighted by a red box. The view is planar for all the graphs similar to this one. The manifold trajectories also have a third dimension, but it is not shown here for simplicity, and because it is small when measured in the EM rotating plane. Note that some of the conditions highlighted in the graph on the left overlap when represented in the graph on the right. The colours of the trajectories are related to the point on the periodic orbit they depart from, i.e., the value of phase angle θ, as in the colour map reported in Fig. 3. The blue area shows the ZVCs of

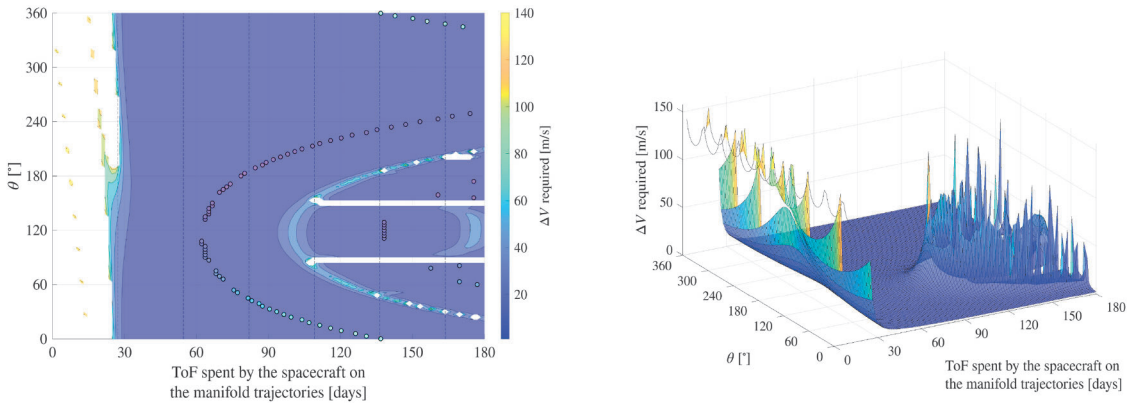

Fig. 6. Disposal cost analysis results for a single orbit - EM-L_2 Halo, $JC = 3.1480$. Disposal ΔV as a function of the phase angle and the time the satellite spends on the manifold before performing the second disposal manoeuvre. Left: 2D view. Right: 3D view.

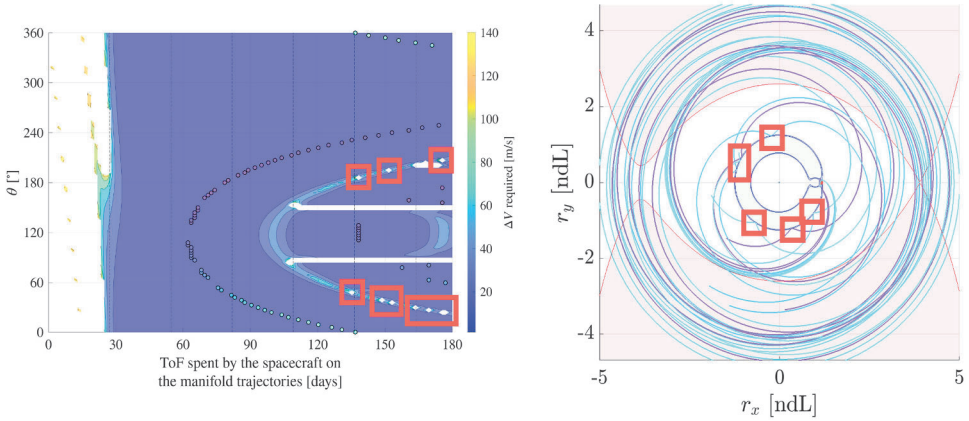

Fig. 7. Representation of some conditions where disposal is not feasible. Case 1: the trajectory crosses the ZVCs of EM-L_2 when far from EM-L_2. Left side: disposal ΔV as a function of the phase angle and the time the satellite spends on the manifold before performing the second disposal manoeuvre; the conditions of interest are highlighted. Right side: trajectories of interest in the EM rotating reference frame; the conditions of interest are highlighted.

the EM system for $JC = JC_{L_2}$, the green area those for a JC equal to that of the reference periodic orbit, and the red area those of the SE system for a JC equal to that of SE-L_2. EM-L_2 is represented as a red dot. It is important to note that the SE ZVCs are shown in the graph solely to provide a qualitative estimate of the distance from the EM-CoM reached by the manifold propagated in EM-CR3BP. The relative position of EM-L_2 and SE-L_2 varies in time, and with them, the relative position of the ZVCs of the two systems. The graph identifies an instantaneous condition, in which the SE ZVCs representation is just qualitative. It is also reasonable to assume that, beyond a certain distance from the EM system barycentre, the CR3BP approximation loses validity. Especially in such cases, incorporating the Sun's gravitational influence becomes necessary to model the dynamics with acceptable accuracy. Nevertheless, all the solutions obtained are considered in this analysis to provide a comprehensive overview of the dynamics governing escape trajectories in the EM system. The inclusion of the Sun's gravitational perturbation in the model is planned for future work.

The conditions observed in Fig. 7 can occur because the ZVCs computed for a JC equal to that of the periodic orbit are slightly narrower than those calculated for a JC equal to that of EM-L_2. This is always true in the cases considered, being the JC of the orbit and hence of the manifold less than that of EM-L_2 if escape trajectories are to be designed. When this condition occurs, the ZVCs cannot be closed, resulting in a locally empty region in the cost plot.

- For some values of θ, unstable manifolds stretching from the periodic orbits exit from EM-L_2, but then re-enter the neighbourhood of the EM system, making disposal unachievable. This is shown by Fig. 8.

  This behaviour is well known and is precisely the reason why a second manoeuvre to close the ZVCs at L_2 is necessary for this type of disposal to be considered effective. Two of the trajectories corresponding to the conditions of interest are highlighted by red boxes, as they re-enter cislunar space and remain within its inner region for the entire remaining propagation time. By contrast, conditions that re-enter and exit cislunar space are highlighted in orange. Both scenarios must be avoided. Ideally, disposal options that are too close to these should also be avoided to ensure that re-entry is reliably prevented. When considering the condition highlighted in orange, any disposal option that occurs after a re-entry in the inner region of the ZVCs should not be considered as a viable option, as such a disposal trajectory could compromise the safety of other missions orbiting cislunar space.

Going back to the analysis of the minimum ΔV conditions, in the left panel of Fig. 9, escape trajectories are shown in the EM non-dimensional rotating frame, propagated for a time equal to $t_{\Delta V_{2min}}$, the time such that, given a certain θ, the condition where the ΔV is minimum is reached.

In the left side of Fig. 9, the final point of each trajectory, which corresponds to the point where the minimum ΔV_2 must be applied to close the ZVCs, is indicated by a coloured dot. Colours of both dots

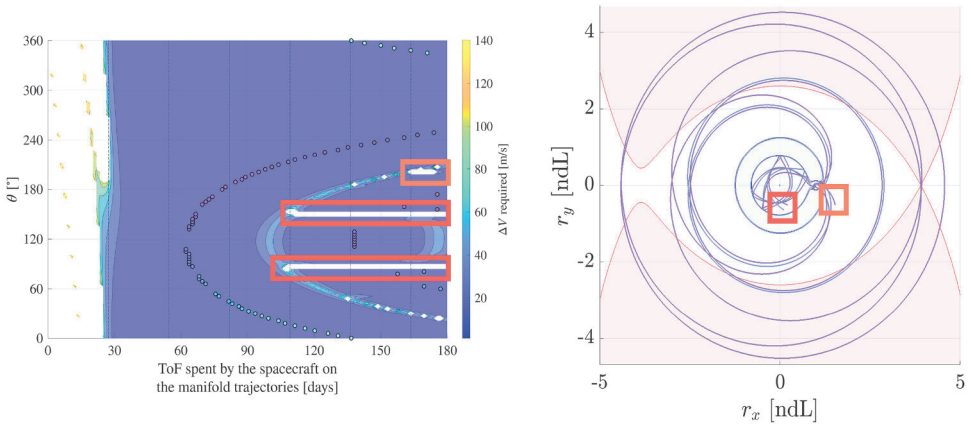

Fig. 8. Representation of some conditions where disposal is not feasible. Case 2: the trajectory re-enters the ZVCs at EM-L_2. Left side: disposal ΔV as a function of the phase angle and the time the satellite spends on the manifold before performing the second disposal manoeuvre; the conditions of interest are highlighted. Right side: trajectories of interest in the EM rotating reference frame; the conditions of interest are highlighted.

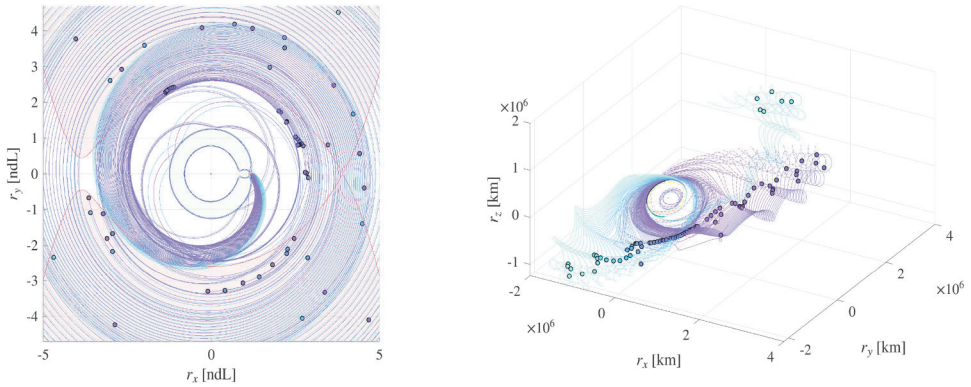

Fig. 9. Left: Escape trajectories in the EM rotating frame. Right: Escape trajectories in the Earth-centred inertial J2000 reference frame.

and trajectories are related to the colour map defined in Fig. 3, and associated with the minimum ΔV found as θ varies.

The trajectories shown in Fig. 9 exhibit a spiral-like pattern, moving progressively away from the centre of the rotating frame as the time corresponding to the minimum ΔV manoeuvre increases. The same disposal trajectories are also displayed in the Earth-centred inertial mean equator and equinox of the J2000 reference frame on the right side of Fig. 9. The transformation between the EM rotating frame and the J2000 reference frame is carried out similarly to what is described in [26]. It is important to note that the transformation is ephemeris-based, i.e., it is time-dependent, and accounts for the roto-pulsating effects arising both from the rotation of the EM reference frame with respect to the inertial one and from the time-varying distance between the Earth and the Moon. The states of all celestial bodies are retrieved at a certain given ephemeris time via the DE440 kernel of the NASA SPICE [27] toolkit. The initial date considered for the propagation is March 8th, 2025. The solid lines represent manifold trajectories before the lowest-cost ZVCs closure condition, while the dashed lines correspond to those after it. The Moon's trajectory is depicted as a solid yellow line. Note that the evolution of the trajectories is shown for the six-month overall propagation time frame in this case. The dashed trajectory visible in the vicinity of the Earth, inside the Moon's orbit, is one of those shown in Fig. 8, re-entering the ZVCs of the EM system if the ZVCs closure manoeuvre is not performed. The colours of the dots and of the trajectories follow the same colour map associated with θ, as defined in Section 3. Observing the two graphs in the Figure, a relationship is hypothesised between the distance of the manifold from the system's CoM and the conditions that lead to the minimum ΔV disposal options. In Fig. 10, the evolution of the distance between the EM system CoM and an object orbiting on the manifold is shown as a function of $t_{\Delta V_2}$.

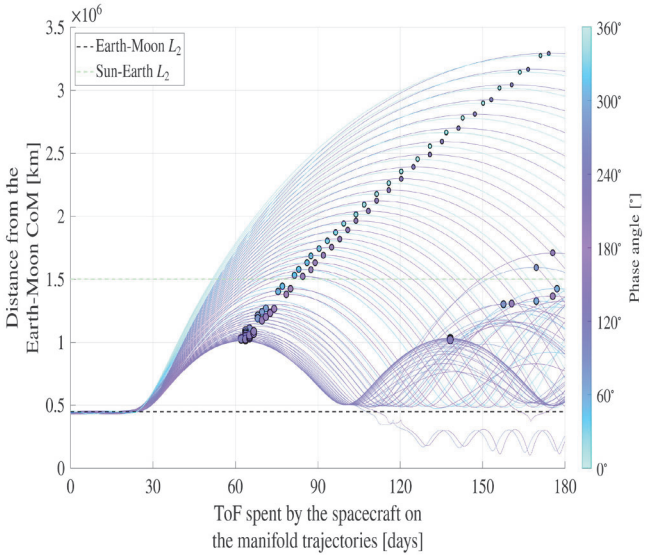

Fig. 10. Evolution over time of the distance between the manifold and the EM system CoM.

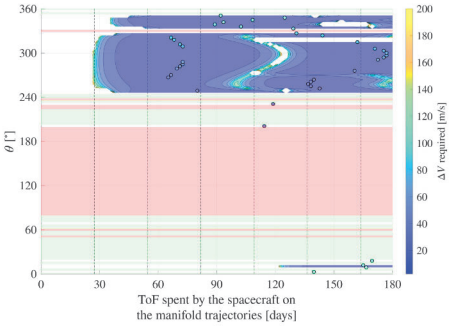

(a) Disposal ΔV as a function of the phase angle and the time the satellite spends on the manifold before performing the second disposal manoeuvre - 2D view.

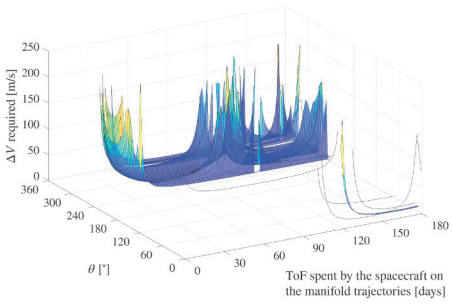

(b) Disposal ΔV as a function of the phase angle and the time the satellite spends on the manifold before performing the second disposal manoeuvre - 3D view.

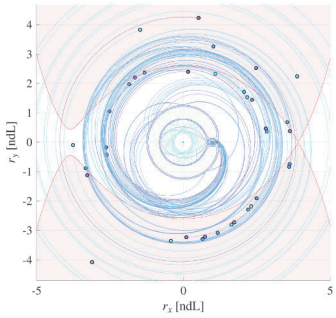

(c) Escape trajectories in the EM rotating frame.

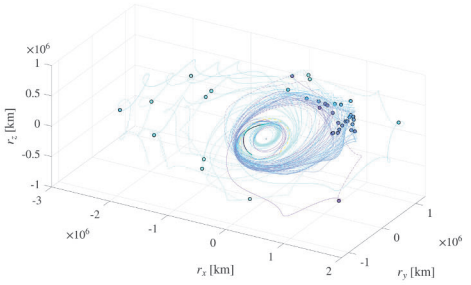

(d) Escape trajectories in the Earth-centred inertial J2000 reference frame.

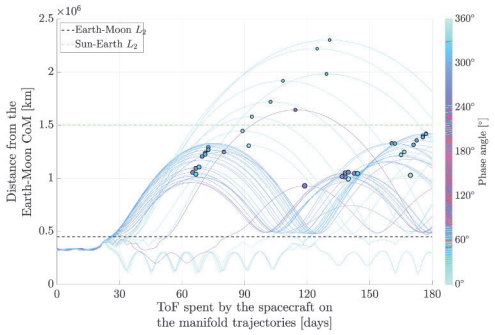

(e) Evolution over time of the distance between the manifold and the EM system CoM.

Fig. 11. Analysis of no-return trajectories escaping from EM-L_2, originating from a Halo orbit in EM-L_1 ($JC = 3.1208$).

In Fig. 10, the dots indicate the minimum ΔV disposal conditions. Their size reflects the relative magnitude of the required minimum ΔV across all values of θ considered. Two key trends can be observed. First, the minimum ΔV always occurs when the satellite is at the apocentre of the manifold with respect to the EM CoM. Secondly, the disposal cost generally tends to decrease as the apocentre increases. Indeed, the cost of the disposal manoeuvre appears to be primarily influenced by the magnitude of the apocentre radius of the manifold and its relative position with respect to the EM system's CoM. This can also be verified from Eq. (9): for a constant JC, smaller values of ΔV_2 are required where the local velocity of the object along the manifold is lower, i.e., near the apocentre. Conditions for which the minimum-ΔV solution would occur at $t_{\Delta V_{2,\min}} \geq 6$ months are not included in the graph.

Referring to the previously mentioned conditions where, for high values of $t_{\Delta V_2}$, disposal was not feasible, it is also interesting to note that this behaviour can be observed in Fig. 10 as well. Such conditions are those where the distance between the manifold and the EM system's CoM is lower than or close to that of EM-L_2 for high values of $t_{\Delta V_2}$: when the manifold crosses the ZVCs of the EM system evaluated at L_2, whose mean radius is slightly greater than the EM-L_2 distance, or re-enters the ZVCs at L_2, disposal is not feasible.

5.2. *Halo in L_1, southern branch*

The same analysis proposed in the previous Subsection for one Halo orbit in L_2 is proposed herein for one Halo orbit in L_1 with $JC = 3.1208$. As a general consideration, what was described with respect to L_2 Halo orbits is valid in this case and all the others as well. The results are shown in Fig. 11.

Analysing these results, it is evident how disposal is generally more challenging for orbits around L_1. However, the overall considerations remain consistent with those previously discussed for L_2 Halo orbits. In

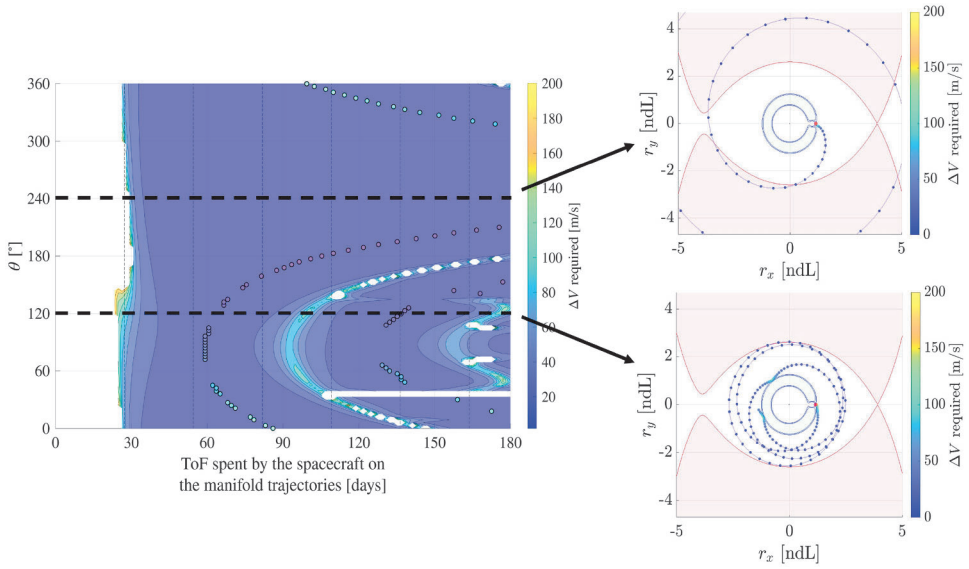

Fig. 12. Disposal ΔV evolution against trajectory evolution, $\theta = 120°$ and $\theta = 240°$. L_2 Halo with $JC = 3.1287$.

the graphs showing the ΔV evolution, the trajectories of the manifolds that impact the Moon, intersect the GEO belt or remain within cislunar space for the entire period considered are identified with different colours, i.e., red, black and green respectively.

5.3. Behaviours in the evolution of escape trajectories

Observing the evolution of escape trajectories in the EM rotating reference frame and that of the distance of the manifold from the system CoM for the two reference orbits analysed, it is interesting to note that:

- Some of the trajectories exhibit an almost periodic evolution of the distance from the system CoM once they are outside EM-L_2. This almost periodic behaviour is of interest because it could somehow resemble Keplerian dynamics, with clearly defined apocentre and pericentre radii. These trajectories are also the ones where the CR3BP approximation is particularly adequate, since the distance from the EM CoM remains bounded. In such cases, the minimum ΔV required for disposal is high with respect to others, but still reasonable from the operational point of view, while the $t_{\Delta V_{2min}}$ is low.
- For some of the trajectories, instead, the distance from the EM-CoM increases exponentially, and no clear periodic behaviour is observed. In other words, a periodic behaviour is present, but with a longer period than what is observed in the previous cases. These cases are such that the manifolds' apocentre is reached for high values of $t_{\Delta V_{2min}}$, and low ΔV values are generally required for disposal. It is fair to say, however, that these are the cases for which it is difficult to assume the CR3BP approximation would hold.

To describe this concept also from another point of view, the evolution of the disposal cost is plotted against some of the trajectories analysed. As an example, the L_2 Halo orbit with $JC = 3.1287$ is selected. The ΔV budget evolution along two disposal trajectories, corresponding to two different initial phase angle values, $\theta = 120°$ and $\theta = 240°$, is shown in Fig. 12.

In Fig. 12, the evolution of the disposal ΔV is plotted against the manifold one for two specific values of the phase angle θ. All the possible disposal points considered are displayed and coloured according to the same colour map used for the ΔV evolution shown in the graph on the left. For $\theta = 240°$, the ΔV reaches a maximum for low $t_{\Delta V_2}$ values but then consistently decreases as $t_{\Delta V_2}$ increases. This behaviour is also reflected in the trajectory evolution, which, following a spiralling-like pattern, progressively moves away from the EM system CoM, with the ΔV required for disposal gradually decreasing as the distance from the EM CoM increases. Instead, for $\theta = 120°$, the evolution of the ΔV on the left graph crosses some "islands" where the ΔV is higher compared to what is observed for lower $t_{\Delta V_2}$ values. This is also reflected in the graph on the right, where such evolution is shown against that of the manifold trajectory. The regions where ΔV is high for high $t_{\Delta V_2}$ correspond to those for which the manifold approaches the ZVCs of EM-L_2, reaching what can be identified as a pericenter in the trajectory evolution.

It is evident that, in general, escape trajectories exhibit principally two types of behaviour:

- An oscillatory behaviour, where apocentres and pericentres are progressively reached;
- A spiral-like behaviour, where the distance from the EM CoM progressively increases as $t_{\Delta V_2}$ increases.

To help explain why some trajectories display one behaviour instead of the other, EM-L_2 escape manifold trajectories are propagated for two months and shown in the left-most graph of Fig. 13.

In the middle graph of the Figure, some of these same trajectories are shown colour-coded: blue for those exhibiting an oscillating behaviour, and red for those following a spiral-like behaviour. When a propagation time of only two months is considered, this difference is not yet evident, but it emerges when longer propagation times are chosen, as in the graph on the right where the manifold is propagated for three months.

From this comparison, two important considerations can be drawn:

- Trajectories in the manifold that oscillate around the system's CoM without moving far from it are the ones that, for short propagation times, reach limited distances from the EM CoM, remaining closer to it than trajectories that display a spiral-like behaviour. The latter, instead, are those that reach greater distances from the EM CoM right from the beginning.
- The distinction between these two behaviours becomes evident once the manifold has completed more than one relative revolution around the system's CoM. This occurs because the six-month time frame is significantly longer than the characteristic dynamical timescales of the EM system. By considering such an extended period, behaviours that would never appear over shorter time spans are highlighted.

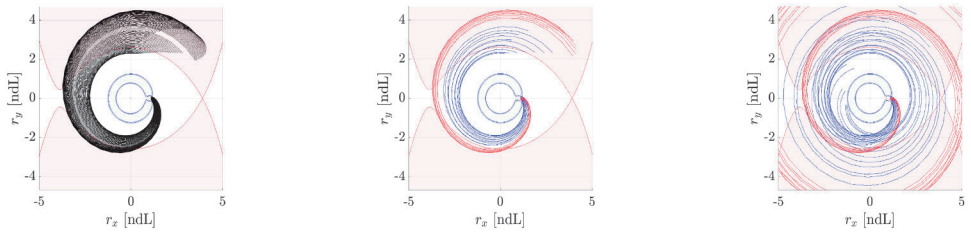

Fig. 13. Manifold trajectories behaviour, L_2 Halo with $JC = 3.1287$. From left to right: EM-L_2 escape manifold trajectories propagated for 2 months. EM-L_2 escape manifold trajectories propagated for 2 months, colour coded. EM-L_2 escape manifold trajectories propagated for 3 months, colour coded. All trajectories are shown in the EM rotating frame. Colour code: blue, trajectories showing an oscillating behaviour when longer $t_{\Delta V_2}$ are considered; red, trajectories showing a spiralling behaviour when longer $t_{\Delta V_2}$ are considered. (For interpretation of the references to colour in this figure legend, the reader is referred to the web version of this article.). (For interpretation of the references to colour in this figure legend, the reader is referred to the web version of this article.)

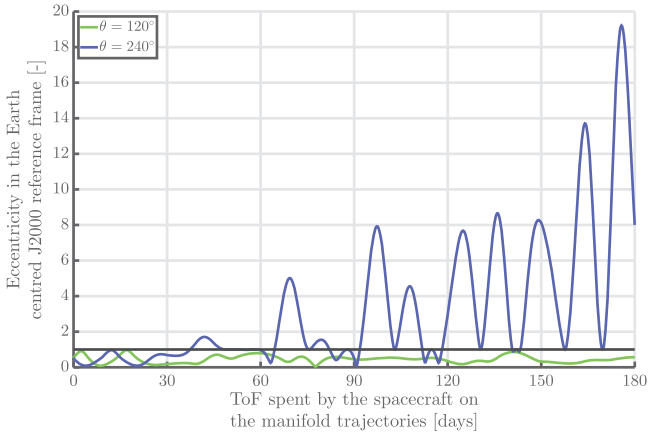

Fig. 14. Eccentricity evolution over time for two escape trajectories, $\theta = 120°$ and $\theta = 240°$. L_2 Halo with $JC = 3.1287$.

Moreover, in Fig. 14, the evolution of the geocentric eccentricity over time, evaluated in the J2000 reference frame, is shown for the two trajectories identified in Fig. 12. The dashed black line in the graph identifies an eccentricity equal to 1.

The evolution of the eccentricity associated with the spiralling-like trajectory, corresponding to $\theta = 240°$, is similar to that of hyperbolic-like Keplerian trajectories, reaching values well above 1. The eccentricity of the trajectory associated with the oscillatory behaviour, $\theta = 120°$, remains instead below 1 throughout the entire propagation time, showing a trend more similar to that of parabolic Keplerian orbits. What is particularly noteworthy is that, although the difference between the two behaviours becomes fully evident only when observing the entire timespan, the spiralling-like trajectory already reaches an eccentricity greater than 1 after about 40 days. This means that the distinction between the two behaviours can be identified from the very beginning of the propagation, without the need for long-term simulations.

To confirm what has been discussed, the same behaviour is shown in the ΔV evolution for the L_2 Halo with $JC = 3.0669$, another time for $\theta = 120°$ and $\theta = 240°$, shown in Fig. 15.

Also in this case, the evolution of the ΔV is shown together with that of the trajectory in the EM rotating reference frame for two phase angles, $\theta = 120°$ and $\theta = 240°$. For $\theta = 240°$, the cost is high at the beginning and then decreases as $t_{\Delta V_2}$ increases, and the trajectory exhibits a spiralling-like behaviour. Instead, for $\theta = 120°$, the disposal ΔV evolution passes through regions on the left plot where the required ΔV is high for high $t_{\Delta V_2}$. Also in this case, the trajectory evolution shows how these high ΔV regions are associated with the pericenters of the disposal trajectory. These are also the points where the manifold approaches the EM-L_2 ZVCs. The two behaviours characteristic of the manifolds' evolution are also shown for this orbit, in Fig. 16, together with the eccentricity evolution for the two selected trajectories, in Fig. 17.

The same conclusions drawn for the previous case can be confirmed: the behaviour of the trajectories is mainly influenced by the distance they reach from the EM CoM from the very beginning of the propagation and by the evolution of their eccentricity. Note that, in this case, the oscillatory-type trajectory, corresponding to $\theta = 240°$, reaches eccentricity values slightly above 1 at the beginning of the propagation, but this occurs before the escape from EM-L_2 takes place (see the cost graph in Fig. 15). This kind of behaviour, likely related to the presence of the Moon and to the trajectory evolution before escape, could be further investigated in future work.

6. Parametric analysis results

The method described in the previous Sections has been applied to all the candidate orbits considered. This has made it possible to carry out a parametric study aimed to investigate how the minimum ΔV required to insert a spacecraft onto an escape no-return trajectory, ΔV_{min}, and the corresponding ToF spent by the spacecraft on the manifold before performing the ZVCs closure manoeuvre, $t_{\Delta V_{2min}}$, vary as functions of the orbits' JC and the manifold insertion point's phase angle, θ. The ΔV is defined as the sum of $||\boldsymbol{\Delta V_1}||$ and $||\boldsymbol{\Delta V_2}||$.The following subsections present and discuss the parametric analysis results for each orbital family in turn, comparing the results obtained.

6.1. Halo in L_2, southern branch

The results for the parametric analysis on the southern branch of the L_2 Halo family are reported in Fig. 18. The graph shows the evolution of two key parameters: ΔV_{min} and $t_{\Delta V_{2min}}$, as a function of the orbits' JC and the manifold insertion point's phase angle, θ.

On the left side of the Figure, the evolution of $t_{\Delta V_{2min}}$, the ToF during which the spacecraft follows the unstable manifold before the ZVCs closure manoeuvre, is shown as a function of θ and the JC. On the right side, the evolution of the ΔV_{min} is shown as a function of the same parameters. Values for which $\Delta V_{\text{min}} > 50\,m/s$ are discarded, as they are considered not significant for this analysis. A disposal ΔV budget greater than $50\,m/s$ could be considered excessive for a cislunar mission, and it is therefore reasonable to focus only on conditions that meet this threshold. Consequently, conditions such that $\Delta V_{\text{min}} > 50\,m/s$ are excluded from the colour bar that relates the disposal cost evolution to the two parameters of interest, and are identified by a deep purple colour.

The empty spaces in the graphs correspond to conditions for which, to reach the minimum ΔV, it would be necessary to wait for a period longer than six months. This does not imply that disposal is not feasible under those conditions, but rather that the unstable manifold, for those specific values of θ and JC, reaches a position where the ΔV

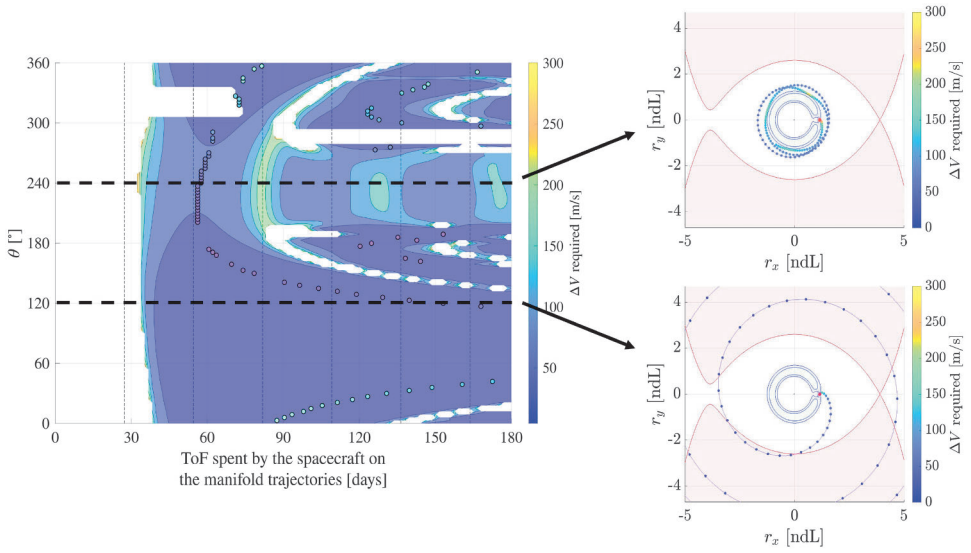

Fig. 15. Disposal ΔV evolution against trajectory evolution, $\theta = 120°$ and $\theta = 240°$. L_2 Halo with $JC = 3.0669$.

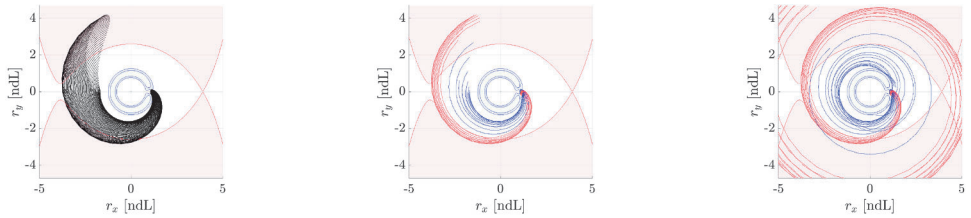

Fig. 16. Manifold trajectories behaviour, L_2 Halo with $JC = 3.0669$. From left to right: EM-L_2 escape manifold trajectories propagated for 2 months. EM-L_2 escape manifold trajectories propagated for 2 months, colour coded. EM-L_2 escape manifold trajectories propagated for 3 months, colour coded. All trajectories are shown in the EM rotating frame. Colour code: blue, trajectories showing an oscillating behaviour when longer $t_{\Delta V_2}$ are considered; red, trajectories showing a spiralling behaviour when longer $t_{\Delta V_2}$ are considered. (For interpretation of the references to colour in this figure legend, the reader is referred to the web version of this article.). (For interpretation of the references to colour in this figure legend, the reader is referred to the web version of this article.)

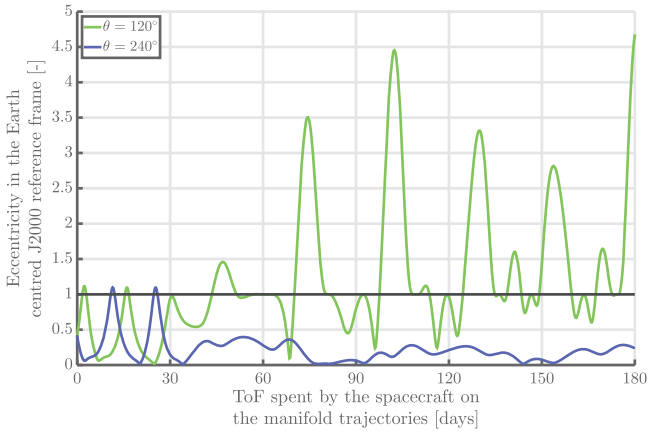

Fig. 17. Eccentricity evolution over time for two escape trajectories, $\theta = 120°$ and $\theta = 240°$. L_2 Halo with $JC = 3.0669$.

is minimum for $t_{\Delta V_{2\min}} \geq 6$ months. Neglecting these conditions in the subsequent analysis means excluding a portion of the available solution space. This is, of course, an approximation, as it may imply removing solutions that could potentially offer even lower ΔV values than those shown in Fig. 18 if a higher limit on the ToF is taken into account. However, this is considered reasonable, given the operational significance of the six-month limit. These cases will be studied in future work by including the influence of the Sun in the model, which becomes essential given the distances from the EM system CoM that these trajectories reach.

No conditions are found in which the manifold trajectories intersect a region of space with a radius comparable to that of the GEO belt around the Earth, $r_{GEO} \simeq 42000$ km. Instead, fewer than ten conditions are found where the manifold trajectories do not cross EM-L_2 within six months, remaining constrained inside cislunar space for the overall period considered. These are identified by a bright green colour and occur only for low JC values. The same is true for lunar impacts, identified by red. To facilitate the interpretation of these cases, a legend is provided at the top of each graph. Categories are included in the legend only when they actually appear in the parametric analysis results for the corresponding family.

The right side of the graph, where the JC is higher, shows a less chaotic evolution in both $t_{\Delta V_{2min}}$ and $\Delta V_{\min}$ when compared to the left side of the graph, where the JC is lower. This latter region corresponds to orbits closer to the Moon and with lower stability indices, i.e., which are more stable, than those with higher JCs, as shown in Fig. 4. As detailed in Section 3, the JC decreases with the stability index, i.e., as the linear stability of the orbit increases, and with the perilune radius across all families considered. Additionally, as the JC decreases, the number of low-cost solutions becomes smaller. This occurs both because the greater the difference between the orbital energy level and that of L_2, the greater the effort required to bridge the gap needed to close

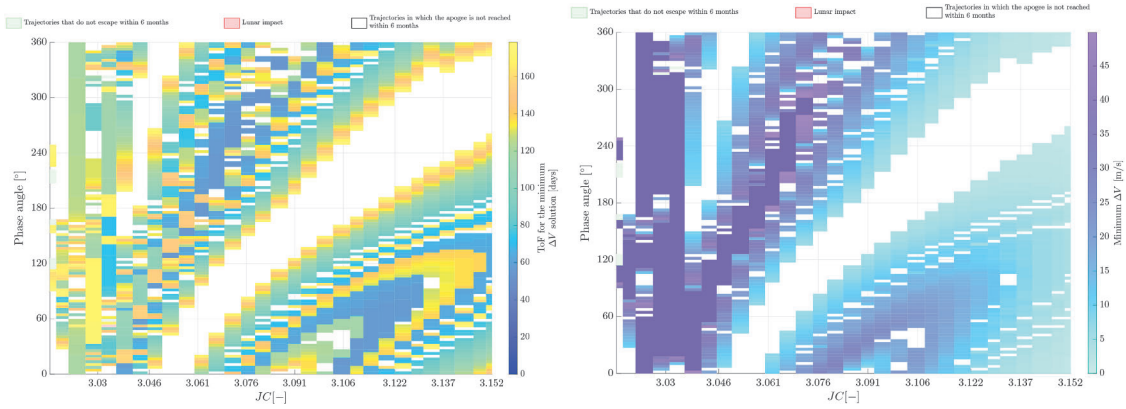

Fig. 18. Parametric analysis results. Evolution of the ToF of the solution with minimum ΔV (left) and of its minimum ΔV (right) as a function of the orbits' JC and the manifold insertion point's phase angle — Southern L_2 Halo family.

the ZVCs, and because, even when low cost solutions are found, they correspond to conditions in which higher apogees are reached more slowly than in solutions involving a comparable ΔV and departing from orbits with a higher JC. Consequently, as a general rule, no-return trajectories are more convenient as a disposal option for L_2 Halo orbits with high values of JC. Going back to analysing the graphs, it is interesting to note that:

- Especially for high JCs, given a fixed energy value, and thus a specific reference periodic orbit, it is sufficient to apply the impulse ΔV_1 at a precise value of θ to successfully insert the spacecraft into escape trajectories requiring limited costs and ToFs.
- From an operational standpoint, it is reasonable to assume a mission would have fixed constraints on the maximum ΔV and ToF allowed for the disposal phase. The maps shown in Fig. 18 can be used to identify particular conditions within the orbital family that satisfy fixed cost and ToF requirements. Even if such conditions do not belong to the operational orbit associated with the hypothetical mission, future work would investigate heteroclinic and homoclinic connections between different periodic orbits that, at low cost, could enable the transfer of satellites from their operational orbits to some more favourable from a disposal ΔV budget point of view.
- There exist conditions under which, even for significantly different values of phase angle and energy, the results obtained in terms of $t_{\Delta V_{2min}}$ and $\Delta V_{\min}$ are comparable. This may imply that some solutions may be geometrically similar.

To analyse this last point, four conditions with similar $t_{\Delta V_{2min}}$ are selected, and the related analyses are presented in Fig. 19.

The four conditions selected are indicated on the map by dark green dots. Each of these conditions corresponds to a specific L_2 Halo orbit, characterised by a fixed JC value, i.e., energy level. The four JC values selected, from left to right on the x-axis of the map, are $JC = 3.0575$, $JC = 3.0669$, $JC = 3.1287$ and $JC = 3.1480$. The four specific conditions, all having a ToF of about 50 days, are also highlighted on the graphs placed around the map with dark green boxes.

When considering all the graphs showing the disposal cost evolution (four of them shown in Fig. 19), it is important to note that the limits of the colour map representing the required ΔV trends have not been fixed across different orbits. This choice was made to make it easier to observe how the cost evolves for each orbit individually, but it could make comparing graphs of different orbits more complex. In any case, the minimum disposal costs required for the various orbits are all consistently compared in Fig. 18.

In Fig. 19, the four selected cases shown are characterised by similar values of $t_{\Delta V_{2min}}$; however, when examining the graphs in the highlighted boxes, the only evident similarity among the four conditions is that the apocenter radius of the manifold trajectories is always relatively close to the EM-L_2 distance, with respect to what is found for other minimum ΔV conditions. Additionally, all disposal points are located on the opposite side of the x-axis with respect to L_2, a factor that might be favourable for disposal if low ToFs are desired and specific values of θ can be selected to apply the first impulse to the spacecraft and place it on the desired manifold trajectory. Nonetheless, this cannot be established as a general rule, since this trend is not consistently observed across all the cases analysed. Moreover, it is worth noting that some of the $\Delta V_{\min}$ conditions are found near EM-L_2 for higher values of $t_{\Delta V_{2min}}$. This situation is not ideal, since perturbations to the CR3BP dynamics could significantly alter the trajectory's path, making it reasonable to hypothesise a potential re-entry into cislunar space if the ZVCs closure manoeuvre is planned too close to EM-L_2.

It is also important to note that although the four cases considered have similar values of $t_{\Delta V_{2min}}$, they exhibit significantly different values of $\Delta V_{\min}$. Specifically, for the two cases on the right ofFigure 19, the required $\Delta V_{\min}$ is relatively low, whereas for the two on the left, it is particularly high. This difference can be attributed to the fact that the manifold evolution becomes much more chaotic when lower JCs are considered. This, which was expected and has been briefly discussed earlier, becomes especially evident when examining the middle graph of each box, in which the evolution of the manifold trajectories is represented up to the point where the minimum ΔV ZVCs closure manoeuvre would be performed. The increased chaotic nature of the trajectories complicates the disposal process as JC lowers, making it more expensive in terms of required ΔV budget (particularly when targeting low $t_{\Delta V_{2min}}$ values) and more challenging to interpret from a dynamical perspective.

Also a second representation, similar to that in Fig. 19 is proposed, selecting this second time two cases with low and similar values of $t_{\Delta V_{2min}}$, and two with high and similar values of $t_{\Delta V_{2min}}$. The reference orbits chosen for this analysis have $JC = 3.0287$, $JC = 3.0669$ (present also in Fig. 19), $JC = 3.1246$, and $JC = 3.1480$ (present also in Fig. 19).

In Fig. 20, the two cases requiring high $t_{\Delta V_{2min}}$ s are identified by red dots and boxes, the two requiring low $t_{\Delta V_{2min}}$ s by green dots and boxes. It is also important to consider that, for the two cases on the right of Fig. 20 (high JCs), the ΔV is low, for the two cases on the right (low JCs), the ΔV is high. All the trends described previously are confirmed when comparing these last four cases as well. It is important to note how, for both cases with high $t_{\Delta V_{2min}}$, the distance between the point where the disposal manoeuvre is performed and the EM system's CoM is relatively low compared to that reached by other trajectories of the manifold. This shows that high values of $t_{\Delta V_{2min}}$ do not necessarily correspond to high distances from the EM CoM at the disposal point. This is true only for cases where the disposal cost is initially high and then uniformly decreases as $t_{\Delta V_2}$ increases. In cases like those selected here, where the

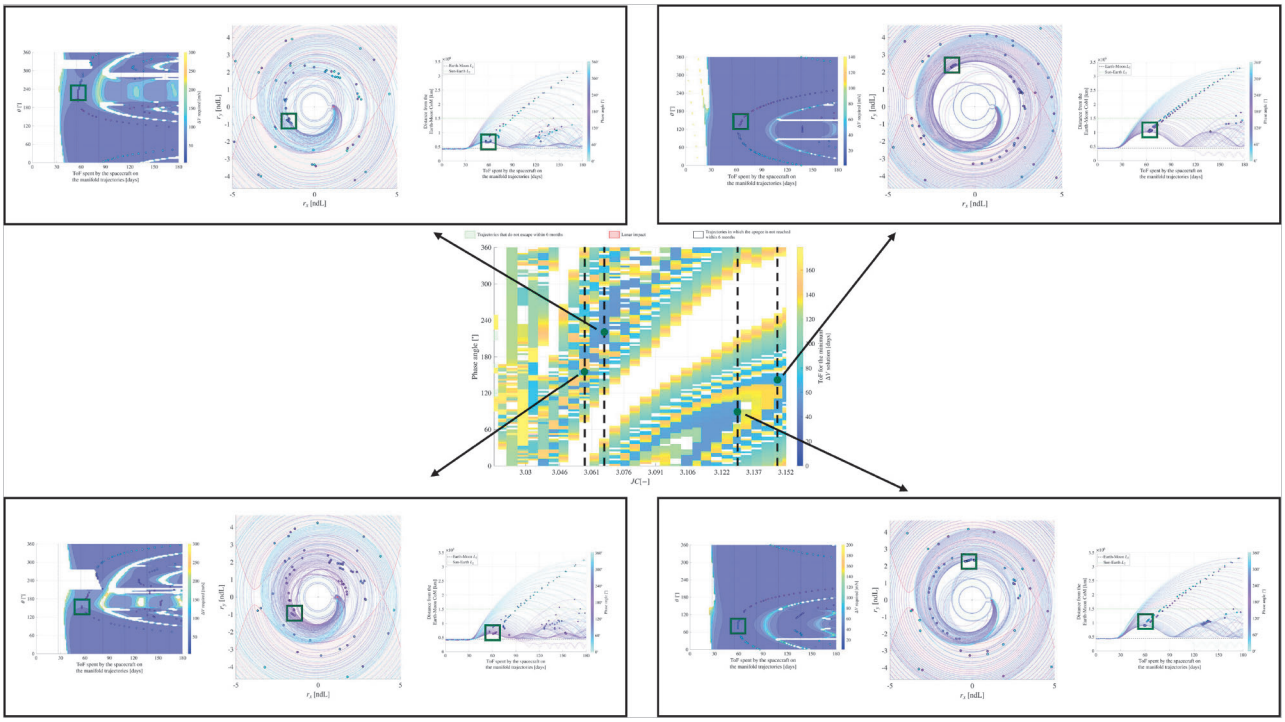

Fig. 19. Behaviour of four different solutions with similar values of $t_{\Delta V_{2min}}$.

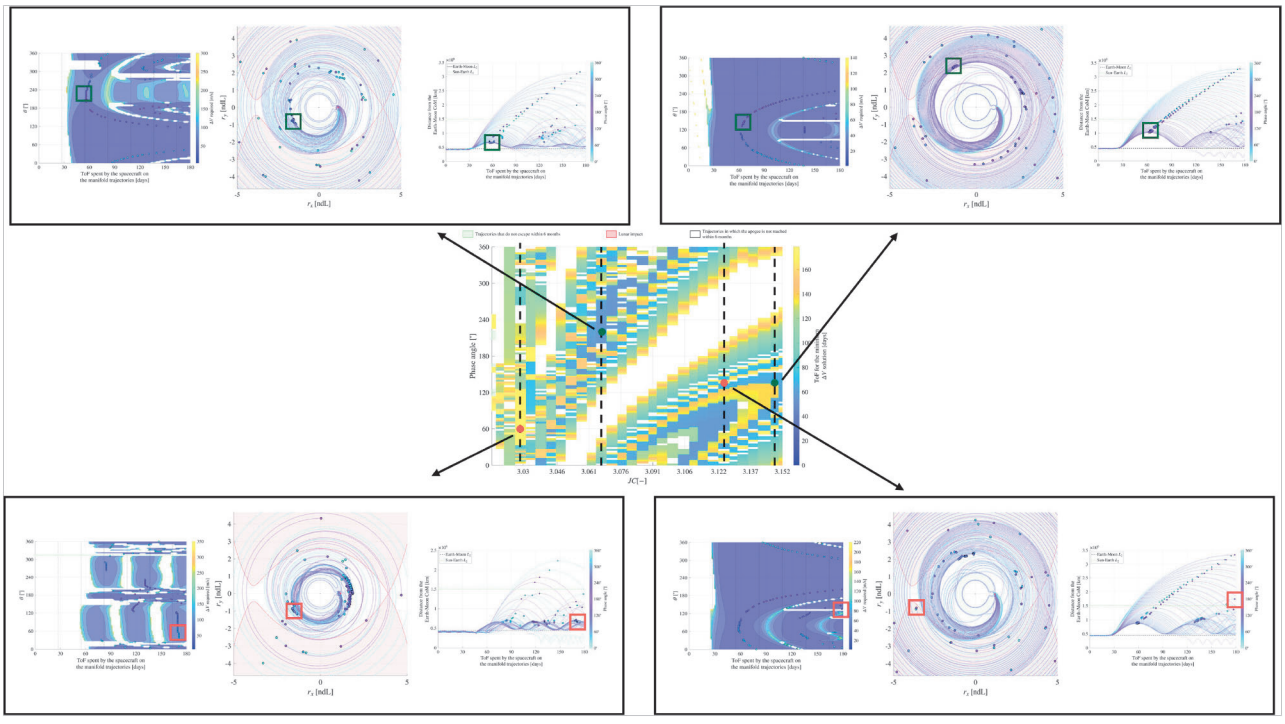

Fig. 20. Behaviour of four different solutions, two with similarly high values of $t_{\Delta V_{2min}}$, and two with similarly low values of $t_{\Delta V_{2min}}$ - L_2 Halo, southern branch.

disposal cost oscillates over time, there can be situations where the condition for performing the lowest-cost disposal is found at a relatively short distance from the system's CoM.

Another interesting aspect that can be observed in Figs. 19 and 20 is that a certain form of symmetry can be identified in the escape behaviour and in the maps of the parametric analysis, even though it is not always centred at the same value of θ. For example, in the upper right panel of Fig. 20, the minimum ΔV evolution exhibits a parabola-like shape, with a vertex slightly below 120°, with respect to which the trajectories' evolution is symmetric (since a minimum ΔV condition corresponds to an apocentre). The same behaviour can be recognised in the central map reporting the results of the parametric analysis: the "phase space-like" central region of the plot identifies the symmetry centres of the trajectory evolutions, whose position shifts as the JC varies (in this case approaching 0° or 360° as it decreases). Thus, a form of symmetry with respect to θ is identifiable in the results, at least when the system

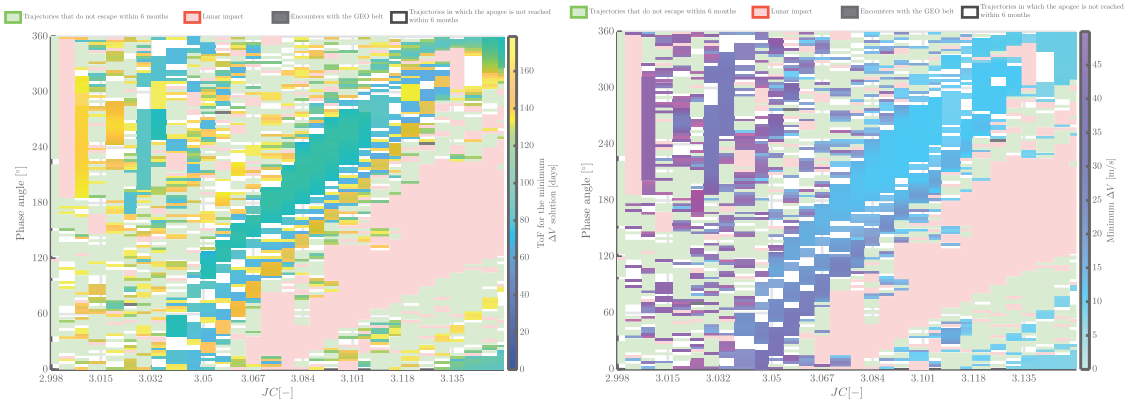

Fig. 21. Parametric analysis results. Evolution of the ToF for the solution with minimum ΔV (left) and of its minimum ΔV (right) as a function of the phase angle and Jacobi Constant — Southern L_1 Halo family.

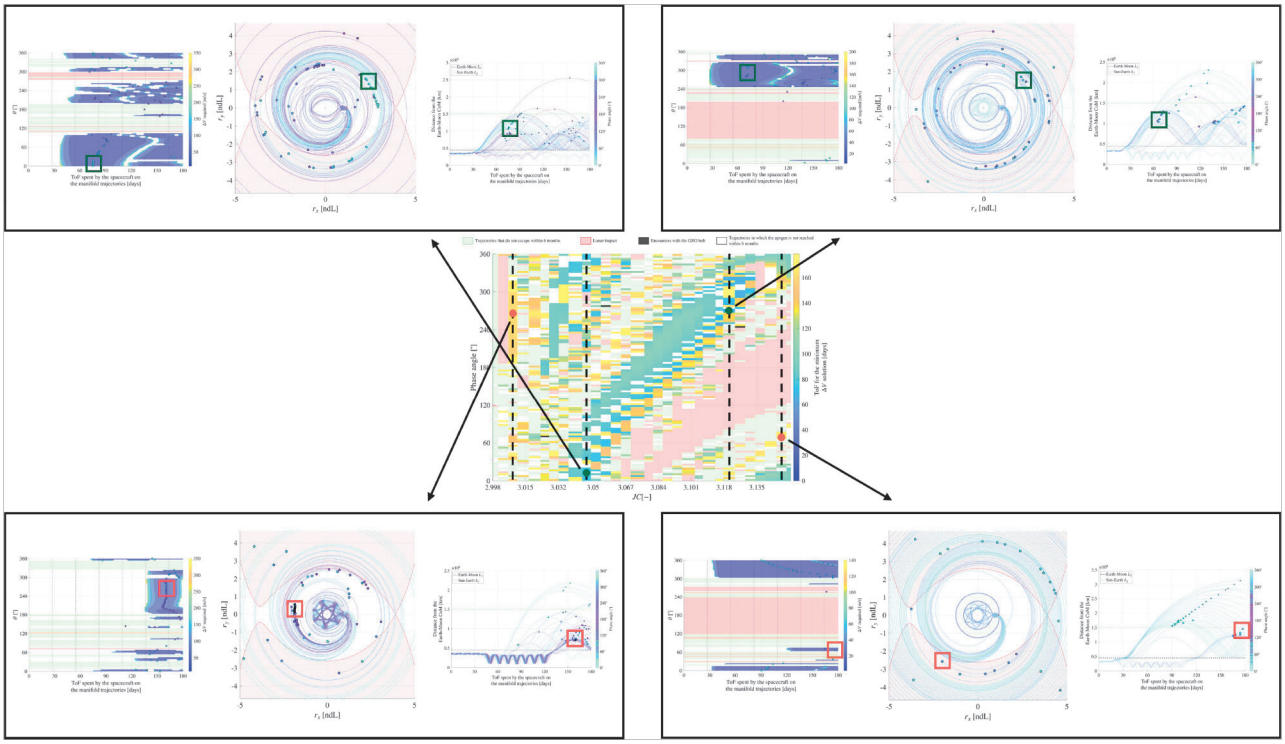

Fig. 22. Behaviour of four different solutions, two with similarly high values of $t_{\Delta V_{2min}}$, and two with similarly low values of $t_{\Delta V_{2min}}$ - L_1 Halo, southern branch.

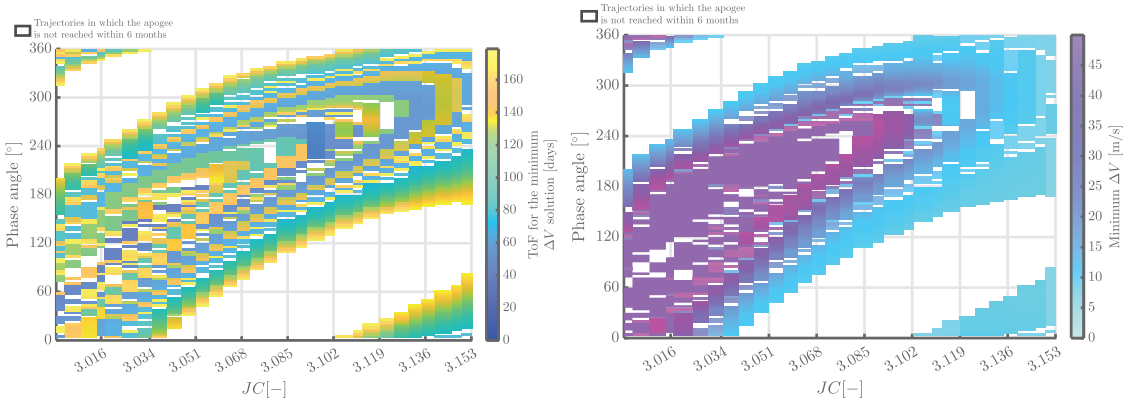

Fig. 23. Parametric analysis results. Evolution of the ToF for the solution with minimum ΔV (left) and of its minimum ΔV (right) as a function of the phase angle and Jacobi Constant — L_2 Lyapunov family.

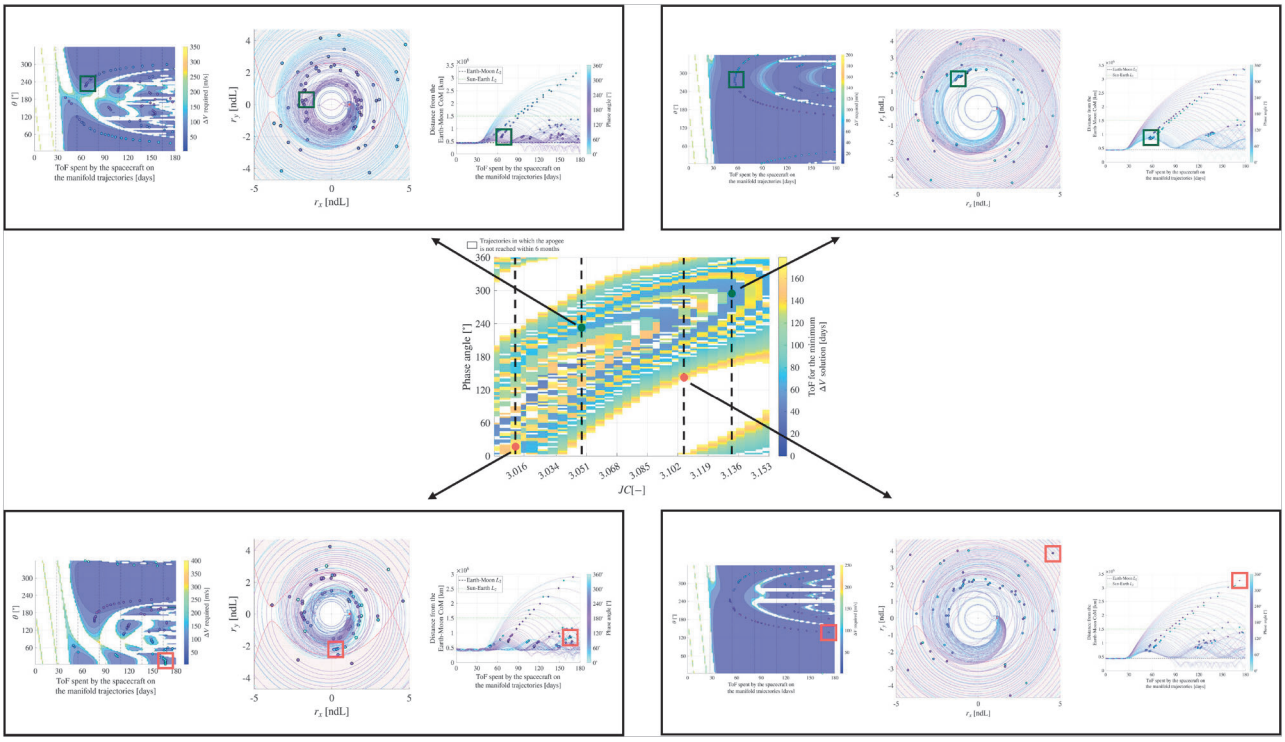

Fig. 24. Behaviour of four different solutions, two with similarly high values of $t_{\Delta V_{2min}}$, and two with similarly low values of $t_{\Delta V_{2min}}$ - L_2 Lyapunov.

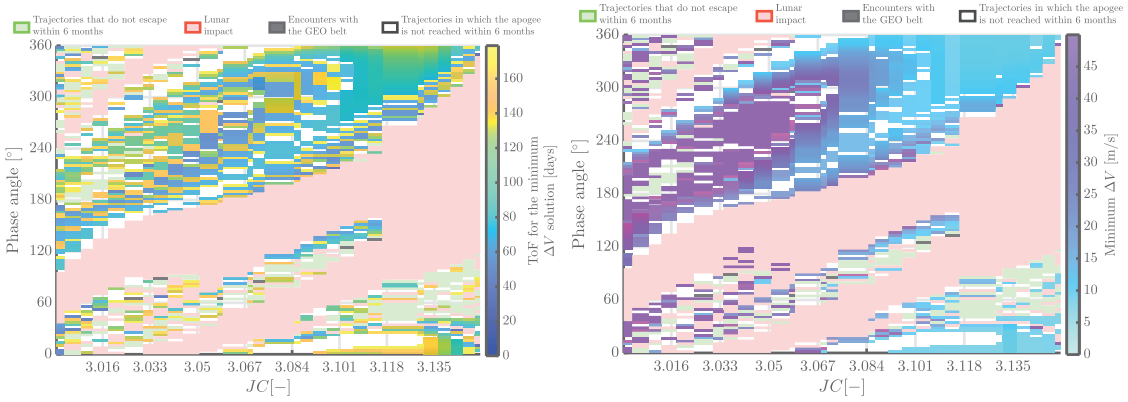

Fig. 25. Parametric analysis results. Evolution of the ToF for the solution with minimum ΔV (left) and of its minimum ΔV (right) as a function of the phase angle and Jacobi Constant — L_1 Lyapunov family.

is not in strongly non-linear regimes, although it is not always centred at the same value. This occurs because the perturbation ε used to inject the spacecraft from the periodic orbit onto the unstable manifold is not tuned for each orbit, but is kept constant for all cases considered. A different choice of ε would correspond to a rotation of θ, and it is reasonable to assume that properly adjusting ε to the characteristics of each initial periodic orbit could yield symmetry centres located at similar conditions across the entire family.

As a final comment, it should be noted how the discussion related to the southern branch of the L_2 Halo orbits has been extensive and detailed. The majority of the behaviours highlighted are also valid for all the other families analysed; therefore, to avoid unnecessary repetition, such a detailed analysis will not be presented for them. When differences arise compared to what has been discussed for the L_2 Halo orbits, they will be clearly emphasised. Otherwise, the conclusions and evaluations made for this family should be considered valid for the others as well.

6.2. *Halo in L_1, southern branch*

The results of the parametric analysis for the southern L_1 Halo family are shown in Fig. 21.

For the L_1 Halo family, disposal through no-return escape trajectories generally proves more complicated with respect to what was observed for the L_2 Halo family. This is expected, since it is reasonably more challenging for orbits with L_1 as their equilibrium point to cross cislunar space and reach EM-L_2. Many conditions that lead to an uncontrolled impact on the Moon are found and identified by red areas in the graphs. Therefore, as a general rule, the risk of uncontrolled Moon impacts is high when choosing this kind of disposal for L_1 Halo orbits, apart from some particular combinations of JC and initial phase angle, where, since they are found in the middle of successful disposal "isles" in the graphs, using this kind of strategy seems feasible. At the same time, many conditions exist in which the spacecraft does not cross EM-L_2 for the entire six-month period, never exiting cislunar space: these are

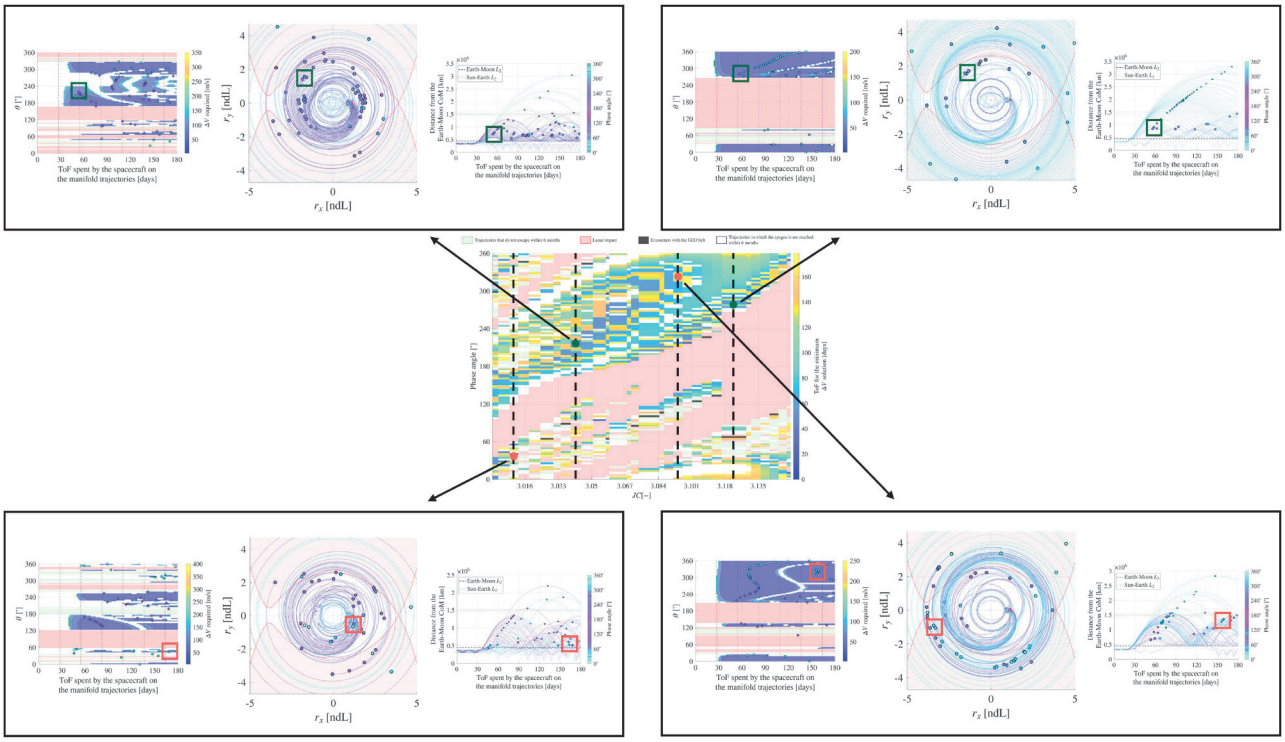

Fig. 26. Behaviour of four different solutions, two with similarly high values of $t_{\Delta V_{2min}}$, and two with similarly low values of $t_{\Delta V_{2min}}$ - L_1 Lyapunov.

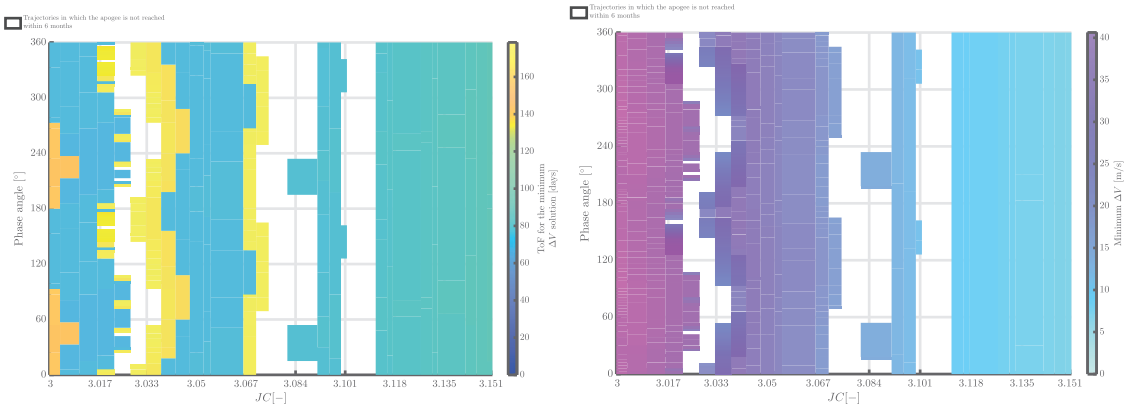

Fig. 27. Parametric analysis results. Evolution of the ToF for the solution with minimum ΔV (left) and of its minimum ΔV (right) as a function of the phase angle and Jacobi Constant — L_2 Vertical family.

shown in bright green. By contrast, only a few manifold trajectories, shown in black, intersect the region of space around the Earth with a radius equal to that of the GEO belt.

As shown for the L_2 Halo family, disposal appears difficult to achieve for low JC values, whereas some of the conditions identified for high JC values seem more promising. As with the L_2 Halo family, orbits characterised by low JC values are unstable but have a higher tendency towards linear stability compared to those with high JC values. This confirms that a greater linear stability is related to an increasingly challenging disposal design, as far as no-return disposal trajectories and the L_2 and L_1 Halo families are considered.

Another interesting observation is that the pattern resulting from this parametric analysis appears almost complementary to that obtained for L_2 Halo orbits. Specifically, when considering orbits at a given JC level, the values of initial phase angle θ for which achieving minimum disposal ΔV conditions would take longer than six months for an L_2 Halo orbit are the same for which, for an L_1 Halo orbit, disposal is instead achievable within a reasonable time frame, i.e., $\Delta V_{\text{min}} \sim 10$ m/s and $t_{\Delta V_{2min}} < 90$ days. This strongly suggests a relationship between the two families and their manifolds, highlighting the presence of heteroclinic connections between them. This is particularly relevant because it opens up opportunities both from a disposal and a trajectory design perspective. For disposal, when operating in a constrained orbit with limited ΔV and time available for EoL manoeuvres, it is possible to evaluate disposal strategies that leverage heteroclinic connections between the two orbital families to meet mission requirements. From a trajectory design point of view, heteroclinic connections between the two families can be exploited to identify low-cost transfer options between some of their members.

Apart from this, the considerations made regarding the results for the parametric analysis on the L_2 Halo family remain valid for the L_1 Halo family as well. In this case too, four conditions are selected for more in-depth analysis, and reported in Fig. 22: two with similarly low $t_{\Delta V_{2min}}$ values, belonging respectively to orbits with $JC = 3.0463$ and

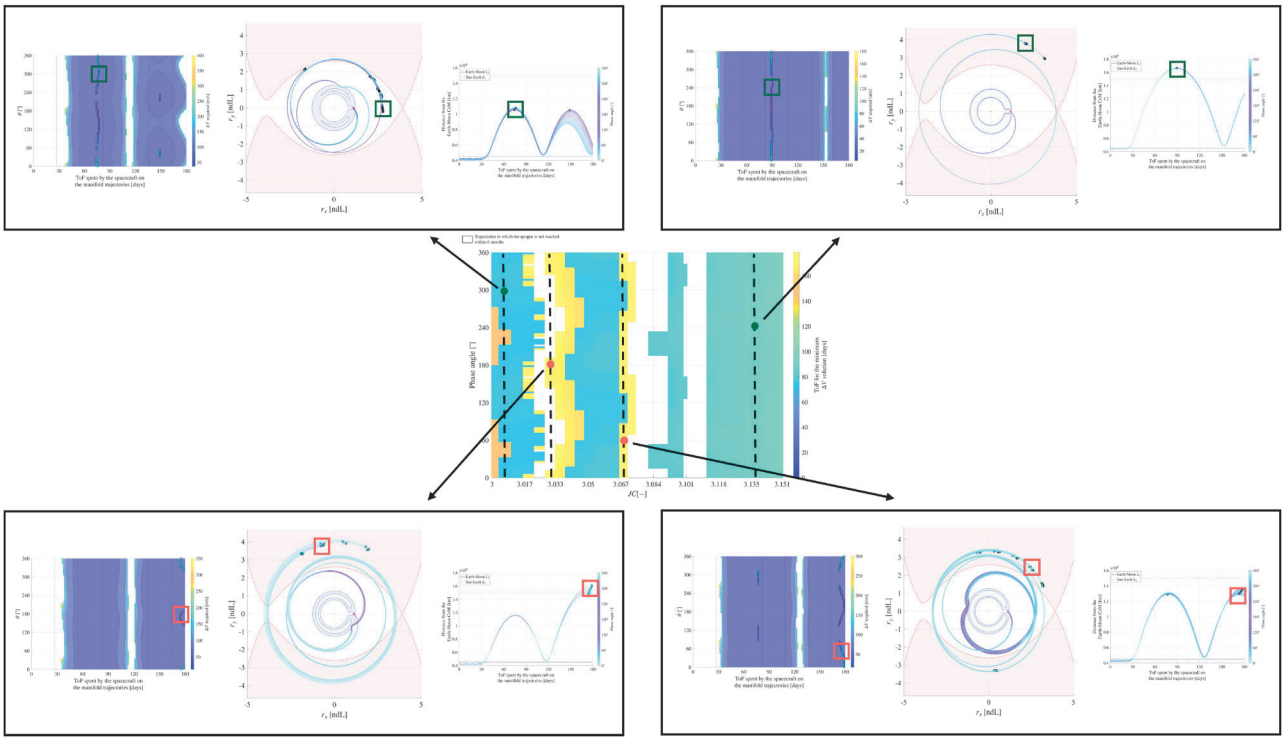

Fig. 28. Behaviour of four different solutions, two with similarly high values of $t_{\Delta V_{2min}}$, and two with similarly low values of $t_{\Delta V_{2min}}$ - L_2 Vertical.

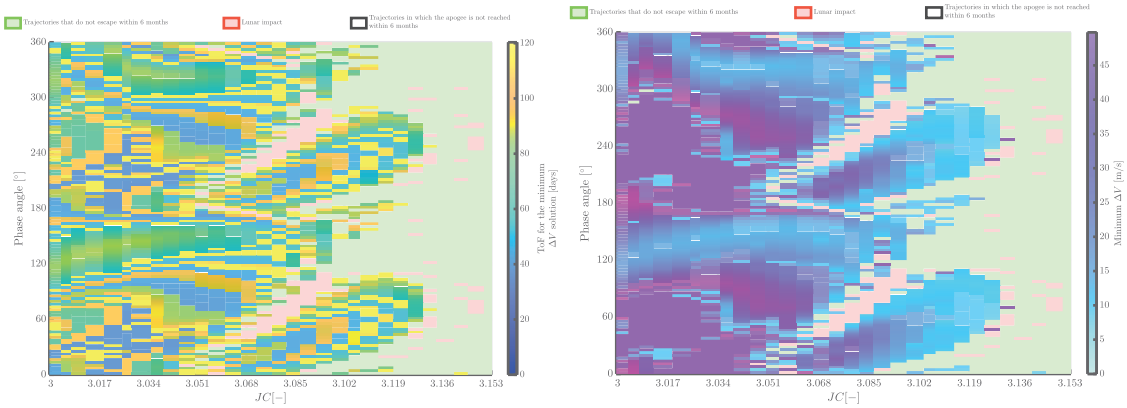

Fig. 29. Parametric analysis results. Evolution of the ToF for the solution with minimum ΔV (left) and of its minimum ΔV (right) as a function of the phase angle and Jacobi Constant — L_1 Vertical family.

$JC = 3.1208$, and two with similarly high $t_{\Delta V_{2min}}$ values, belonging to orbits with $JC = 3.0083$ and $JC = 3.1477$.

Also in this case, the two low $t_{\Delta V_{2min}}$ conditions are identified by green dots and boxes, while the two with high $t_{\Delta V_{2min}}$ values are identified by red dots and boxes. In the cost evolution graphs, where disposal is achievable, low disposal ΔVs are consistently found $15 - 20$ days after escape from L_2. Minimum ΔV conditions are identified, as in the L_2 Halo case, by coloured dots, which follow the colour map associated with the initial phase angle evolution. In this case, however, the parabolic-like shape that maps the combinations of initial phase angle and $t_{\Delta V_2}$ values guaranteeing ΔV_{min} is no longer evident. This is due both to the presence of many cases in which disposal is not feasible, which makes it difficult to identify a clear pattern, and to the increased variety of behaviours exhibited by manifold trajectories. Note that, also in this case, manifold trajectories all follow a similar pattern for low ToFs; however, since they remain in a region characterised by strong non-linear dynamics and significant gravitational influence from both the Earth and the Moon, they exhibit increasingly different behaviours as the ToF progresses.

In the distance evolution graph, it is possible to observe how some manifold trajectories remain inside cislunar space for some time before exiting through EM-L_2 and having the possibility to perform the disposal. This behaviour is also visible in the trajectory evolution plot and in the cost evolution graph. It is related to trajectories with relatively high initial $t_{\Delta V_2}$ values, for example, the case shown in the lower left panel of Fig. 22, for $\theta \sim 10°$. Such conditions are generally not advisable, since they imply that the spacecraft orbits within cislunar space for an extended period before disposal, which is operationally challenging and may pose risks to ongoing missions.

6.3. Lyapunov in L_2

The results of the parametric analysis for the L_2 Lyapunov family are shown in Fig. 23. In Fig. 24, a more complete analysis is shown for

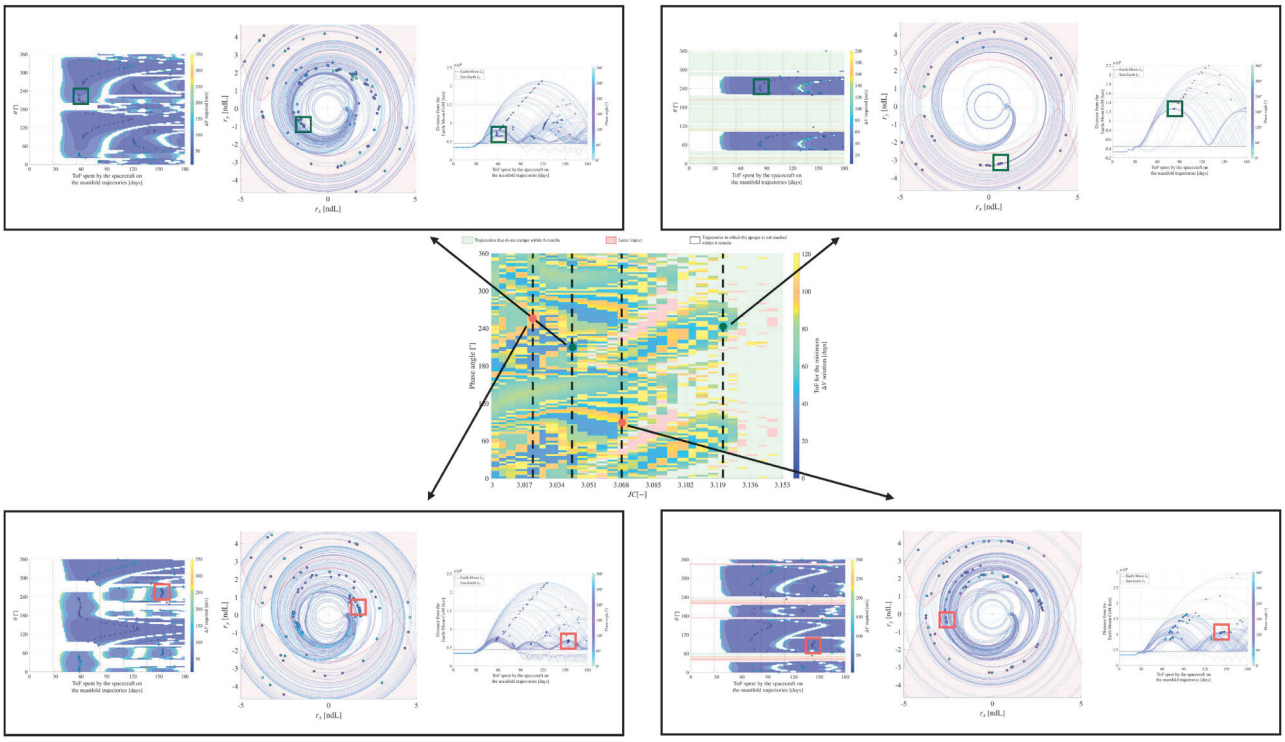

Fig. 30. Behaviour of four different solutions, two with similarly high values of $t_{\Delta V_{2min}}$, and two with similarly low values of $t_{\Delta V_{2min}}$ - L_1 Vertical.

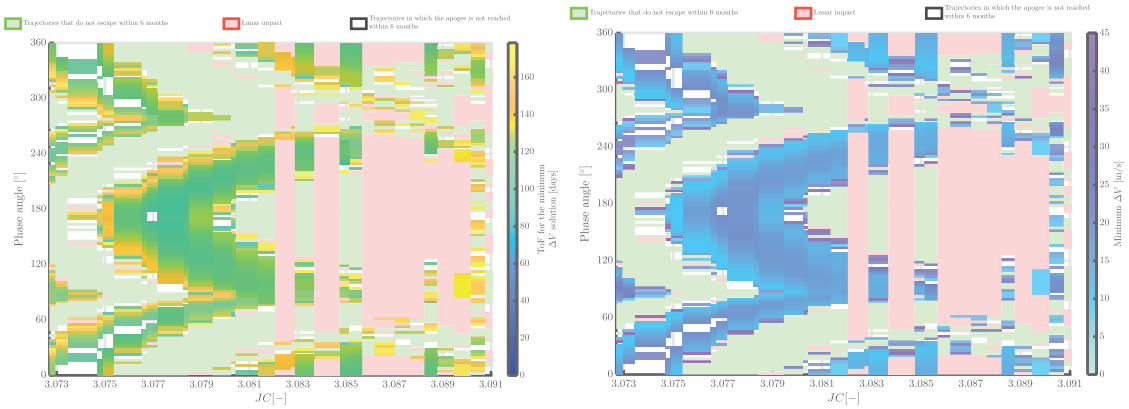

Fig. 31. Parametric analysis results. Evolution of the ToF for the solution with minimum ΔV (left) and of its minimum ΔV (right) as a function of the phase angle and Jacobi Constant — Southern Butterfly family.

four different minimum ΔV cases: two characterised by low $t_{\Delta V_2}$ values, $JC = 3.0482$ and $JC = 3.1321$, and two by high $t_{\Delta V_2}$ values, $JC = 3.0114$ and $JC = 3.1061$.

A pattern similar to that observed for L_2 Halo orbits is found, although with a shift in the results as a function of the angle θ. This can be explained by recalling that the perturbation ϵ applied to transition from the periodic orbit to the unstable manifold is the same for all cases analysed, and it is reasonable to expect that it may lead to different outcomes depending on the family considered, as it is arbitrarily chosen. Apart from this, the pattern appears very similar, which indicates a limited influence of the three-dimensional component on the system. As noted in the previous cases, disposal becomes increasingly difficult to achieve at low cost and within reasonable times as JC decreases, the energy of the reference initial orbit increases, and the behaviour of trajectories before performing the ZVCs closure manoeuvre becomes progressively more chaotic.

6.4. *Lyapunov in* L_1

The results of the parametric analysis for the L_1 Lyapunov family are presented in Fig. 25. As for the other families, the behaviour of four representative solutions is shown in Fig. 26: two cases with low $t_{\Delta V_2}$ values, $JC = 3.0101$ and $JC = 3.1238$, and two cases with high $t_{\Delta V_2}$ values, $JC = 3.0421$ and $JC = 3.0940$.

Also in this case, the results are consistent with the discussion presented earlier. The "isles" identifying conditions for which disposal is successful are not, however, perfectly complementary to those identified for L_2 Lyapunov orbits. In all other respects, considerations very similar to those made for L_1 Halo orbits can be drawn. It is worth noting that, in this case, the number of Moon impacts is significantly higher than in the other cases analysed, including L_1 Halo orbits. A reasonable explanation is that, since L_1 Lyapunov orbits are planar, the unstable manifold trajectories they generate are also entirely planar, thus

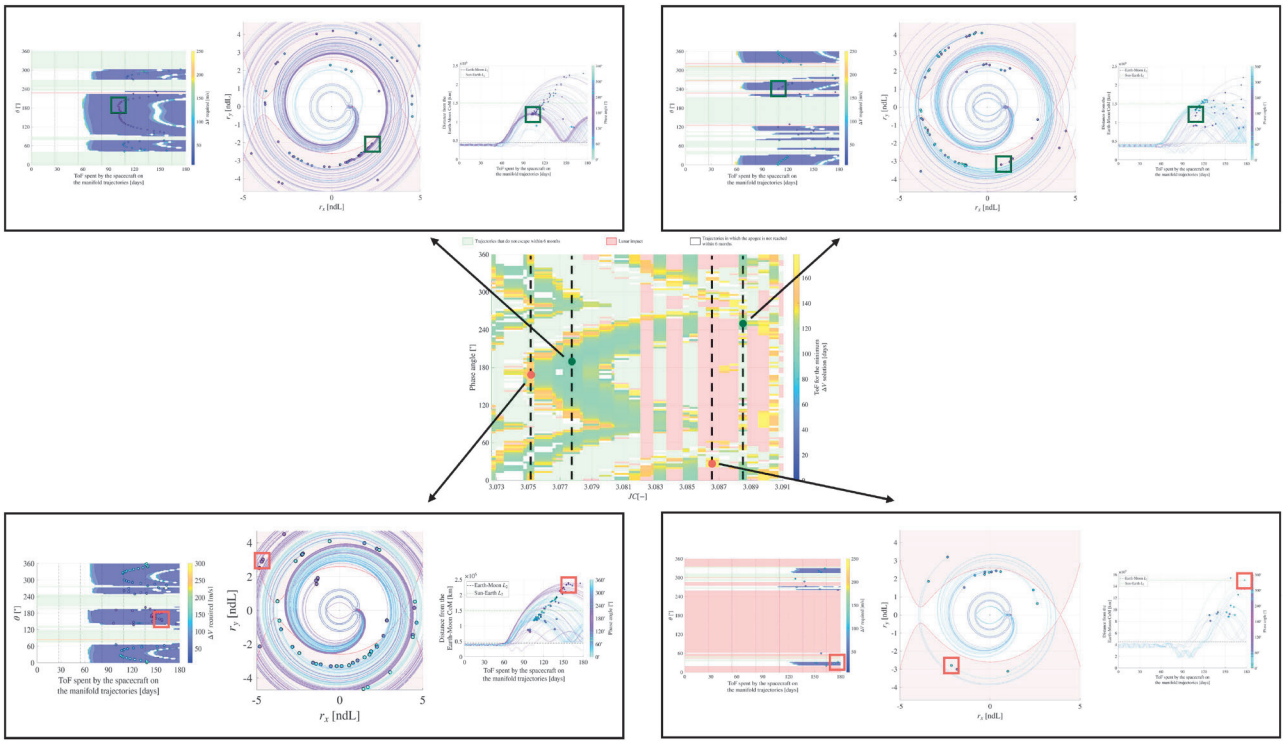

Fig. 32. Behaviour of four different solutions, two with similarly high values of $t_{\Delta V_{2min}}$, and two with similarly low values of $t_{\Delta V_{2min}}$ - Southern Butterfly family.

increasing the probability of intersection between the manifold trajectories and the Moon.

6.5. Vertical in L_2

The results of the parametric analysis for L_2 Vertical orbits are shown in Fig. 27. Four different cases are then reported in Fig. 28: $JC = 3.0065$ and $JC = 3.1365$, with low $t_{\Delta V_2}$, $JC = 3.0301$ and $JC = 3.0683$, with high $t_{\Delta V_2}$.

In the case of L_2 Vertical orbits, the results differ from the usual trend. What is particularly noteworthy is that, in this case, the minimum ΔV disposal cost and corresponding $t_{\Delta V_2}$ do not appear to vary significantly with θ, unlike what was observed in the previous cases, except for a few limited JC values. This occurs because, within the considered JC range, Vertical orbits become progressively farther from L_2 along the z-direction as JC decreases, while remaining in its vicinity in the x and y directions. This indicates that, as also stated before, the position of a point belonging to the orbit along z, r_z, is not a particularly influential parameter for the analysis, since its variation along the orbit consistently yields similar results in terms of both the minimum disposal cost and the disposal duration. Moreover, even when, for a given JC value, the behaviour of the manifold trajectories changes with θ, such variations are not as fragmented as in the previous cases, but instead remain well defined. This can be justified knowing that L_2 Vertical orbits remain much closer to L_2 than to either the Moon or the Earth over the entire JC range considered, meaning that non-linear behaviours, usually more pronounced near one of the two primary bodies, are limited in this case. Additionally, the solutions obtained for θ between 0° and 180° are repeated for phase angles between 180° and 360°. This is an interesting feature, arising from the particular geometry of these orbits and from the way θ is defined in this case: the phase angle spans between 0° ans 180° when indicating the lobe of the orbit with positive r_z, and between 180° and 360° for the lobe with negative r_z. In other words, L_2 Vertical orbits are symmetric with respect to the xy-plane, and this symmetry is clearly reflected in the results. Conversely, while all the orbit families considered are symmetric with respect to the xz-plane, such symmetry does not appear to be evident in the parametric analysis results. Moreover, the fact that identical solutions are obtained as θ varies is also reflected in the manifold trajectories' evolution, since, having fixed a JC value, all trajectories consistently exhibit the same behaviour, as illustrated in the trajectory and distance evolution graphs in Fig. 28. When two distinct types of solutions are found over the entire phase-angle range considered, this is reflected in the trajectory and distance evolution graphs too, as in the case of $JC = 3.0683$ (low-right portion of Fig. 28).

6.6. Vertical in L_1

In Fig. 29, the results of the parametric analysis for L_1 Vertical orbits are presented. Four representative cases are then highlighted in Fig. 30: two characterised by low $t_{\Delta V_{2min}}$ values, namely $JC = 3.0420$ and $JC = 3.1216$, and two characterised by high $t_{\Delta V_{2min}}$ values, namely $JC = 3.0213$ and $JC = 3.0688$.

In this case, the results differ a lot from those obtained for the Vertical family centred in L_2. The values of both $\Delta V_{\min}$ and $t_{\Delta V_{2min}}$ are not constant as θ varies, showing instead a more fragmented profile, similar to what has been observed in all previous cases, except in that of the L_2 Vertical family. As in that case, however, the solutions obtained for θ between 0° and 180° are repeated for θ between 180° and 360°, confirming the previously discussed role of the symmetry with respect to the xy-plane.

The significant discrepancy between the results obtained for the L_2 and L_1 Vertical families can be explained by the fact that escape from the L_2 region is inherently easier for orbits centred in L_2. This effect becomes particularly pronounced for Vertical orbits, due to the following considerations. As can be seen in Fig. 3f and e, the Vertical families in both L_1 and L_2 evolve with significant excursions along the z-dimension and limited variation in the xy-plane. In this case, the parameter that has the greatest influence on escape behaviour is the distance between the escape trajectories' initial points and L_2 projected on the xy-plane. This distance is very low for the L_2 Vertical family overall and very high for the L_1 instead. In other words, when departing from L_1

Table 1
No-return disposal trajectories in the Earth-Moon system: a summary.

Periodic orbit family	General considerations	Minimum ΔV solutions	ToF related to the minimum ΔV solutions
Halo L_2	No-return trajectories appear to be promising disposal options since local solutions requiring both a limited ΔV and ToF are found, particularly for orbits characterised by a high JC, i.e. those that are far from the Moon. Disposal becomes increasingly more difficult the closer one gets to the Moon: for these types of orbits, a controlled lunar impact would probably be more effective.	With high JCs, $\Delta V_{\text{min}} < 15$ m/s, with low JCs, ΔV_{min} ranges between about 7 m/s and 50 m/s.	Very variable across both θ and JC, ranges between approximately 40 days and six months.
Halo L_1	There is a significant risk of impact with the Moon (especially in the case of high JC) or of being unable to escape cislunar space (in the case of low JC). If it is possible to target specific phase angles, no-return escape trajectories should be considered a reasonable disposal option for a specific range of JC, limited to approximately $3.05 - -3.118$.	In the promising range of JCs, for targeted phase angles, it is possible to find conditions such that $\Delta V_{\text{min}} < 15$ m/s. For lower values of JC, ΔV_{min} can reach up to 50 m/s.	In the aforementioned range, the ToF required to reach the minimum ΔV solutions is about $80 - -100$ days.
Lyapunov L_2	Same considerations given for the L_2 Halo family.	With high JCs, $\Delta V_{\text{min}} < 15$ m/s, with low JCs, ΔV_{min} ranges between about 15 m/s and 50 m/s	Same considerations given for the L_2 Halo family.
Lyapunov L_1	There is a significant possibility of an uncontrolled lunar impact; therefore, controlled impacts would probably be a better disposal option. However, as for the L_1 Halo family, targeting specific phase angle values can lead to reasonable results, for JCs between 3.1 and 3.14.	Within the aforementioned range, $\Delta V_{\text{min}} < 15$ m/s; elsewhere, results are really scattered and can reach up to 50 m/s.	In correspondence of the promising JC range, the ToF ranges between $80 - 140$ days. In other parts of the graph, its evolution is instead really scattered, going from about 40 days up to six months.
Vertical L_2	No-return escape trajectories seem to represent a promising disposal option for the L_2 Vertical family. Even for JC values for which the graph representing the evolution of ΔV_{min} and the relative ToF is empty, solutions can be found; the ΔV_{min} condition is simply never reached within the considered time span due to the unstable manifolds evolution. Interestingly, in this case, the results of the analysis are almost always constant with θ. Results obtained for θ between 0° and 180°, are also shown for θ between 180° and 360°.	For periodic orbits with high JC values, ΔV_{min} is between 5 and 15 m/s, and increases with a decreasing JC, reaching a maximum of about 42 m/s.	The ToF related to the ΔV_{min} solutions is approximately 90 days for high JC values. For lower JC values, the ToF increases or decreases depending on the specific value of JC considered.
Vertical L_1	The most promising results are obtained for low values of JC, with some areas in which the minimum velocity $\Delta V_{\text{min}} < 15$ m/s, with a related ToF of about 110 days. For high JC values, the majority of analysed trajectories do not escape the EM system. The range of solutions for theta between 0° and 180° is repeated between 180° and 360°.	For periodic orbits with JC lower than 3.12, if a precise phase angle is targeted, solutions are found with $\Delta V_{\text{min}} < 15$ m/s.	The evolution of the ToF related to the ΔV_{min} solution is very scattered, going from about 60 days to 6 months.
Butterfly	Many impacts on the Moon and non-escape trajectories within the EM system are observed. Nevertheless, some viable solutions are present, meaning that no-return escape trajectories remain a possible disposal option for this family of orbits. The solutions found are symmetric with respect to 180°.	The majority of viable solutions are characterised by a $\Delta V_{\text{min}} < 20$ m/s.	The ToF related to ΔV_{min} solutions is varies between 100 days and six months.

Vertical orbits, escaping from EM–L_2 is considerably more difficult, as a spacecraft must first reach the EM–L_2 region, which lies at a significant distance. Moreover, trajectories departing from L_1 Vertical orbits should also cross a strongly non-linear region of space influenced by the combined gravitational effect of the Earth and Moon before escaping.

It is also worth noting that, for high JC values, successful disposal solutions are rarely found. Nearly all trajectories remain within cislunar space for the entire six-month period, without ever crossing beyond EM-L_2. This behaviour can be explained, just as the opposite trend can be explained for L_2 Vertical orbits, by the small distance between the orbits and the Lagrange point when JC is high.

As JC decreases, the behaviour of the minimum-ΔV solutions becomes more similar to that observed for Lyapunov or Halo orbits in L_1, generally showing a fragmented pattern except for a few "isles" corresponding to specific (JC, θ) combinations. Interestingly, in this case, the number of lunar impacts is lower than that of trajectories that remain confined to cislunar space for the full six months. This may once again be linked to the z-amplitude reached by these orbits: for L_1 Lyapunov orbits, which are planar, the number of lunar impacts is much higher compared to orbits remaining trapped in cislunar space without escaping through EM-L_2.

6.7. Southern butterfly

The results of the parametric analysis for the southern branch of the Butterfly orbits family are presented in Fig. 31. As in all previous cases, four representative solutions are highlighted in Fig. 32: two with low $t_{\Delta V_{2min}}$, $JC = 3.0778$ and $JC = 3.0885$, and two with high $t_{\Delta V_{2min}}$, $JC = 3.0751$ and $JC = 3.0866$.

Before commenting on the results, it is important to note that in this case the JC range considered is narrower than in the previous analyses, while the range of phase angles remains unchanged. Therefore, when comparing with the results obtained for the other orbit families, it is to be considered that only a subset of the JC range shown for the other cases is examined here. The results appear to be almost symmetric with respect to a value slightly below 180°. This symmetry can be attributed to both the definition of the phase angle and the geometry of these orbits, which are symmetric with respect to the xz-plane and to a plane parallel to the yz one and centred on the Moon. For higher JC values, a large number of impacts with the Moon occur, which in this case can be explained by the close relationship between these orbits and the Moon itself, different from the link between the Moon and the other orbit families, which are centred on one of the Lagrange points. Moreover, both the disposal cost and the $t_{\Delta V_{2min}}$ values required are less

sensitive to variations in JC and θ than in the other cases analysed, with only a few local solutions featuring very high or very low $t_{\Delta V_{2min}}$. The evolution of the unstable manifold trajectories follows a trend similar to that observed in previous cases, as shown in Fig. 32.

7. Conclusions and future works

This work addresses the design of a no-return escape trajectory for spacecraft operating on various families of periodic orbits in the EM system. Specifically, the L_2 and L_1 Halo, Lyapunov and Vertical families, together with the Butterfly one, are considered in the analysis. An initial manoeuvre transfers the spacecraft from its nominal periodic orbit onto a trajectory of the associated unstable manifold. The manifold trajectory passes through the EM-L_2 bottleneck region, escaping towards the outer region of the EM ZVCs. Once outside EM-L_2, a second manoeuvre is executed to close the ZVCs of the EM system, theoretically preventing re-entry into its vicinity. These trajectories are therefore classified as L_2 escape no-return trajectories, and are analysed within the simplified dynamical framework of the EM CR3BP.

A parametric analysis is carried out by varying both the JC of the initial periodic orbit and the phase angle of the point from which the spacecraft departs. The main results of this analysis allow the identification of combinations of orbital energy and disposal departure conditions that are particularly favourable in terms of both cost and transfer time. This outcome is especially relevant since, given mission constraints such as the operational periodic orbit, the maximum allowed disposal time, and the available propellant, the parametric analysis enables the selection of feasible escape-like disposal solutions. Moreover, these results may also support the design of low-cost heteroclinic and homoclinic connections between trajectories, leading to even more low-cost disposal or transfer options. It has also been shown how, for a given trajectory on the unstable manifold, the points from which the ZVCs can be closed at minimum cost correspond to the apocenters of the trajectory itself, together with some other insights about the characteristics of escape trajectory behaviours.

Table 1 summarises the main considerations and general figures of merit obtained as a result of the parametric analysis.

As for future works, two considerations are of particular importance:

- While the adopted dynamical model captures key behaviours in the evolution of disposal trajectories, it does not fully represent the system's dynamics. Including an Ephemeris dynamical model in the complete disposal design is essential for refining the results.
- Long-term disposal safety requires not only ensuring that the spacecraft is unable to return to the EM system, but also that it follows a trajectory crossing the SE L_2 bottleneck region, escaping the SE ZVCs, thereby achieving what is commonly referred to as heliocentric disposal.

Accordingly, future work will first extend the dynamical model to include the Sun, focusing on heliocentric disposal in an approximated framework. Subsequently, disposal solutions will be refined, from start to end, within an ephemeris-based dynamical system.

CRediT authorship contribution statement

Mathilda Bolis: Writing – original draft, Methodology, Investigation, Formal analysis, Conceptualization; **Elisa Maria Alessi:** Writing – review & editing, Supervision, Conceptualization; **Camilla Colombo:** Writing – review & editing, Funding acquisition, Conceptualization.

Data availability

Data will be made available on request.

Declaration of competing interest

The authors declare that they have no known competing financial interests or personal relationships that could have appeared to influence the work reported in this paper.

Acknowledgment

This research has received funding as part of the work developed for the agreement n. 2023-37-HH.0 for the project "Attività tecnico-scientifiche di supporto a C-SSA/ISOC e simulazione di architetture di sensori per SST", established between ASI, Italian Space Agency, and POLIMI, Politecnico di Milano.

Appendix A. Periodic orbits selected for the analysis, as a function of the distance from the Moon.

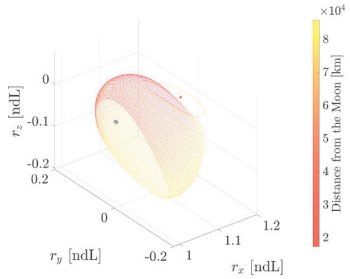

(a) EM-L_2 Halo family, southern branch.

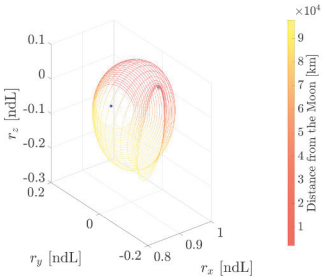

(b) EM-L_1 Halo family, southern branch.

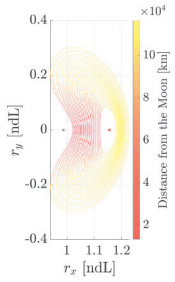

(c) EM-L_2 Lyapunov family.

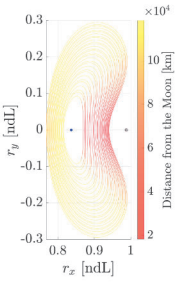

(d) EM-L_1 Lyapunov family.

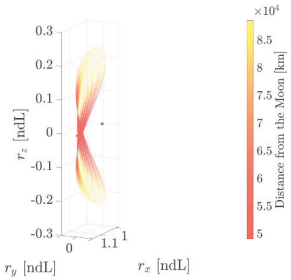

(e) EM-L_2 Vertical family.

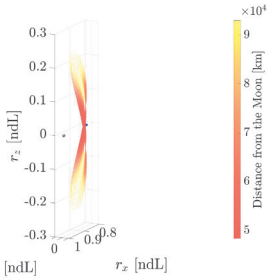

(f) EM-L_1 Vertical family.

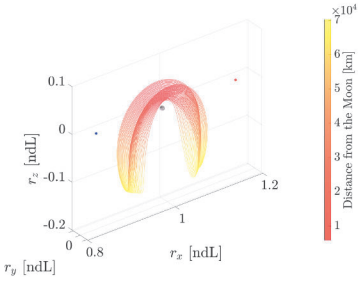

(g) Butterfly family.

Fig. A.33. Periodic orbits selected for the analysis, as a function of the distance from the Moon.

References

[1] M.J. Holzinger, C.C. Chow, P. Garretson, A primer on cislunar space, Tech. rep., Air Force Research Laboratory Greene County, OH, USA, 2021.

[2] ESD Space Debris Office, ESA's annual space environment report, Tech. rep., 2024. No. GEN-DB-LOG-00288-OPS-SD, https://www.sdo.esoc.esa.int/environment_report/Space_Environment_Report_latest.pdf.

[3] A. Black, C. Frueh, Fragmentation characterization in the circular restricted three body problem for cislunar space domain awareness, Adv. Space Res. 75 (1) (2025) 1177–1204. https://doi.org/10.1016/j.asr.2024.08.076

[4] F. Tu, W. Wang, S. Wu, V.Y. Razoumny, Y.N. Razoumny, Optimal control for low-thrust collision avoidance in CRTBP, Aerosp. Sci. Technol. 167 (2025). https://doi.org/10.1016/j.ast.2025.110643

[5] ESA Space Debris Mitigation Working Group, ESA Space Debris Mitigation Requirements, Tech. rep., 2023. Available: ESA Space Debris Mitigation Requirements.

[6] J. Wysack, Cislunar missions end-of-life disposal strategies, in: Advanced Maui Optical and Space Surveillance Technologies Conference (AMOS), Maui, Hawaii, USA, 2024.

[7] M. Nassif, C. Deans, B. Reed, Evaluating disposal and end-of-life strategies for cislunar and lunar missions to enable sustainable exploration, in: AIAA SCITECH Forum, Orlando, Florida, USA, 2025.

[8] S. Bhatiaa, K. Shahb, J. Kamdarc, Review of strategies for cis-lunar space traffic management, in: 73rd International Astronautical Congress (IAC), Paris, France, 2022.

[9] F. Donou-Adonsou, A. Schupp, Yuhas.Patricia, K. Apple, J. Cuddy, J. Loomis, C. Besenfelder, On the lunar missions and post-mission disposal, Space Habitat. 1 (3) (2025). https://doi.org/10.1016/j.spaceh.2025.100030

[10] Z.P. Olikara, G. Gómez, J.J. Masdemont, Dynamic mechanisms for spacecraft disposal from sun-Earth libration points, J. Guid. Contr. Dyn. 38 (10) (2015) 1976–1989. https://doi.org/10.2514/1.G000581

[11] R. Armellin, M. Rasotto, P. Di Lizia, F. Renk, End-of-life disposal of libration point orbit missions: the case of GAIA, Adv. Space Res. 56 (3) (2015) 461–478. https://doi.org/10.1016/j.asr.2015.03.014

[12] C. Colombo, E.M. Alessi, W. Van der Weg, S. Soldini, F. Letizia, M. Vetrisano, M. Vasile, A. Rossi, M. Landgraf, End-of-life disposal concepts for libration point orbit and highly elliptical orbit missions, 110 (2015) 298–312. https://doi.org/10.1016/j.actaastro.2014.11.002

[13] S. Soldini, C. Colombo, S. Walker, The end-of-life disposal of satellites in libration-point orbits using solar radiation pressure, Adv. Space Res. 57 (8) (2016) 1664–1679. https://doi.org/10.1016/j.asr.2015.06.033
[14] K.K. Boudad, K.C. Howell, D.C. Davis, Departure and escape dynamics from the near rectilinear halo orbits in the earth-moon-sun system, J. Astronaut. Sci. 69 (2022) 1076–1114. https://doi.org/10.1007/s40295-022-00328-w
[15] S.T. Scheuerle, D.C. Davis, E.M. Zimovan-Spreen, B.P. McCarthy, D.B. Henry, K.C. Howell, Jettison and disposal from near rectilinear halo orbits, Part 1: theory, in: AAS/AIAA Astrodynamics Specialist Conference, Big Sky, Montana, USA, AAS 23–311, 2023.
[16] D.C. Davis, S.T. Scheuerle, S.L. McCarty, E.M. Zimovan-Spreen, B.P. McCarthy, M.L. McGuire, K.C. Howell, Jettison and disponsal from near rectilinear halo orbits, Part 2: applications, in: AAS/AIAA Astrodynamics Specialist Conference, Big Sky, Montana, USA, AAS 23–306, 2023.
[17] D.C. Davis, K.K. Boudad, S.M. Phillips, K.C. Howell, Disposal, deployment, and debris in near rectilinear halo orbits, in: AAS/AIAA Space Flight Mechanics Meeting, Ka'anapali, Hawaii, USA, 2019.
[18] R.M. Sargent, R.A. Bettinger, C.R. Hartsfield, Preliminary investigation of cislunar disposal reachability via electric propulsion for selected L2 lagrange point orbit families, Discov. Space 129 (2025). https://doi.org/10.1007/s11038-025-09573-z
[19] P. Guardabasso, S. Lizy-Destrez, M. Ansart, Lunar orbital debris mitigation: characterisation of the environment and identification of disposal strategies, in: 8th European Conference on Space Debris (Virtual), 2021.
[20] V. Szebehely, Theory of orbit: the restricted problem of three bodies, Academic Press, 1 edition, 1967. https://doi.org/10.1016/B978-0-12-395732-0.X5001-6
[21] W.S. Koon, M.W. Lo, J.E. Marsden, S.D. Ross, Dynamical systems, the three-body problem and space mission design, Marsden Books, 2011.
[22] E.J. Doedel, V.A. Romanov, R.C. Paffenroth, H.B. Keller, D.J. Dichmann, J. GalÁn-Vioque, A. Vanderbauwhede, Elemental periodic orbits associated with the libration points in the circular restricted 3-body problem, Int. J. Bifurcation Chaos 17 (08) (2007) 2625–2677. https://doi.org/10.1142/S0218127407018671
[23] M. Hénon, Exploration numérique du problème restreint. II. masses égales, stabilité des orbites périodiques, Annales d'Astrophysique, Vol. 28, p. 992 28 (1965) 992.
[24] M. Bolis, Long-term evolution of orbits in cislunar space: characterisation and stability analysis, in: International Astronautical Conference (IAC), Milan, Italy, 2024.
[25] E.M. Zimovan Spreen, Trajectory design and targeting for applications to the exploration program in cislunar space, Ph.D. thesis, School of Aeronautics and Astronautics, Purdue University, 2021.
[26] B. Nicolás Ávila, Invariant manifolds and transport in a Sun-perturbed Earth-Moon system, Ph.D. thesis, Department of Mathematics and Computer Science, University of Barcelona, 2022. Available at: https://hdl.handle.net/2445/190643.
[27] N. SPICE, 2026, avaiable at: https://naif.jpl.nasa.gov/naif/aboutspice.html. Last accessed: 23-03-2026.